SYNTHESIS AND CHARACTERISATION OF $CsBr-Al_2O_3$ COMPOSITE SOLID ELECTROLYTE

by

K. GOPALAKRISHNAN

MATERIALS SCIENCE PROGRAMME

INDIAN INSTITUTE OF TECHNOLOGY KANPUR

April, 1999

SYNTHESIS AND CHARACTERISATION OF $CsBr$-Al_2O_3 COMPOSITE SOLID ELECTROLYTE

A Thesis submitted

in partial fulfillment of the requirement

for the Degree of

Master of Technology

by

K.GOPALAKRISHNAN

to the

MATERIALS SCIENCE PROGRAMME

INDIAN INSTITUTE OF TECHNOLOGY, KANPUR

April 1999

CERTIFICATE

It is Certified that this work on **" Synthesis And Characterisation of CsBr-Al_2O_3 Composite Solid Electrolyte "** by K. Gopalakrishnan has been carried under my supervision and that this has not been submitted elsewhere for a degree.

(K. Shahi)
Professor
Materials Science Programme
I. I. T. Kanpur.

April, 1999

ABSTRACT

Considerable work has been done on Composite Solid Electrolytes (CSEs) since the phenomenon of increase in conductivity due to the dispersion of fine insulating particles in an ionic solid was discovered by Liang in LiI (Al_2O_3) composite system in 1973. Most of the research has revolved around Lithium based ionic compounds. Almost all the models proposed to explain the enhancement in conductivity presume the formation of a space charge layer at the matrix / dispersoid interface. However, the exact mechanism of formation and characterisation of the space charge layer are still subjects of intensive research. The present work was undertaken with a view to contribute to the understanding of the enhancement effect in CSEs and to test the space charge hypothesis.

Mixtures of varying compositions of γ-Al_2O_3 in CsBr were studied. The characterisation was done using DTA, XRD and Complex Impedance Spectroscopy. The maximum enhancement in conductivity was observed for CsBr containing 35 m/o Al_2O_3 of 0.05 μm size. The enhancement was about 18 times that of pure CsBr at 500 $^{\circ}$ C. The Jow and Wagner space charge layer model was found satisfactory to explain the phenomenon .

ACKNOWLEDGMENTS

I express my deep sense of gratitude to Professor K. Shahi, who introduced me to the field of composite solid electrolytes, for his consistent and meticulous guidance throughout the course of the present work.

I am grateful to the staff members of ACMS Dr. Rakesh Bhatnagar, Mr. Umashankar, Mr. U. S. Lal and Mr. Jawar Singh for their technical and non-technical help in the present work.

I would like to thank my colleagues Mr. S. Balasubramanian and Mr. Anshuman Dalvi for their kind cooperation.

Sincere thanks are also expressed to my friends : Balamurugan, Rasmiranjan Samantaray, Manmohan Singh, Sukant Panda and Raja Karthikeyan who made my stay at I. I. T. Kanpur a memorable one.

Gopalakrishnan

CONTENTS

LIST OF FIGURES

LIST OF TABLES

CHAPTER 1

INTRODUCTION

1.1 The Importance Of Solid State Ionics :

Ionic conductivity was first reported by Michael Faraday[1] more than one hundred years ago. The field of "Solid State Ionics" , a term coined by Takehiko Takahashi[2] in the 1960's, deals with the study of the phenomena of ions in solids, especially those which exhibit high ionic or ionic - electronic mixed conductivity at fairly low temperatures below their melting point. It has evolved as an interdisciplinary area of Physics, Electrochemistry and Materials Science. It involves ionic materials having different morphologies which include single crystals, powder specimen and thin films. The increasing interest, in this area of research, during the last few decades maybe attributed to the fact that these materials are inherently leak-proof, electrochemically compatible, rugged, thermodynamically stable and can be miniaturised for many different practical applications in electrochemical devices and power sources.

1.2 Types of Ionic Solids:

It is natural to classify the ionic solids according to the types of defect or disorder responsible for ionic transport[3].These are principally of two types:

(I) Point Defect type

(a) Dilute (less than 10^{18} cm^{-3})

(b) Concentrated (10^{18} - 10^{20} cm^{-3})

(II) Molten Sublattice type (~ 10^{22} cm^{-3})

Solids which exhibit high ionic conductivity and negligible electronic conductivity are called superionic conductors or fast - ionic conductors or solid electrolytes. These belong to the category Ib or II.

1.3. Emerging Areas in Solid State Ionics:

1.3.1. Glasses :

Glassy materials have attracted a great deal of attention because of high ionic conductivity, isotropic nature, absence of grain boundaries, ease of formation, feasibility of obtaining thin films and wide compositional flexibility allowing optimization of electrolytic properties. Usually the ionic conductivity of a glassy solid is 1-2 orders of magnitude greater than its polycrystalline counterpart[4].

Examples : $75AgI.25Ag_2MoO_4$[σ - 1.4 x 10^{-2} $\Omega^{-1}cm^{-1}$ (at 25 ° C)], $44LiI.30Li_2S.26B_2S_3$[σ - 1.6 x 10^{-3} Ω^{-1} cm^{-1} (at 25 ° C)] [5].

1.3.2. Polymers :

Polymer electrolytes have acquired a significant status in the field of Solid State Ionics in view of their interesting properties, such as flexibility, light weight, elasticity and so on offering potential candidates for high energy density batteries.

Example : $(PEG)_{10}LiI$ [σ - 4.1 x 10^{-7} Ω^{-1} cm^{-1} (at 30 ° C)][6].

1.3.3. Composites :

One of the techniques employed to enhance the ionic conductivity of solids is to

Table 1.1.

Some Composite Solid Electrolytes With Enhanced Conductivity:

Composite System	Dipersoid m/o	σ (Ω^{-1} cm^{-1})	$\sigma_{composite}$ / σ_{pure}	at T (° C)
$LiI(Al_2O_3)$[7]	40	$1.0x10^{-5}$	100	25
$CuCl(Al_2O_3)$[8]	10	$2.5x10^{-5}$	30	25
AgI(Fly-Ash)[9]	13.5	$1.2x10^{-5}$	50	25
$AgI(SiO_2)$[9]	10	$1.1x10^{-5}$	45	25
$AgBr(Al_2O_3)$[10]	15	$1.0x10^{-5}$	20	21
$SrCl_2(Al_2O_3)$[11]	25	$7.2x10^{-4}$	5	300
$CaF_2(Al_2O_3)$[12]	4	$5.4x10^{-5}$	100	373
$KCl(Al_2O_3)$[13]	45	$2.1x10^{-5}$	80	300
(0.75AgI:0.25AgCl) (Al_2O_3)[14]	30	$9.2x10^{-4}$	7	27

disperse fine particles of an electrically insulating and chemically inert substance in the ionic compound. Such systems termed are Dispersed Solid Electrolytes Systems. Liang[7] reported the first composite solid electrolyte namely LiI-Al_2O_3, which showed a remarkable enhancement in the Li^+ ion conductivity when Al_2O_3 dispersion was used. Since then, several new composites have been investigated. Table 1.1 lists some of the important Composite Solid Electrolyte Systems which show an appreciable enhancement in conductivity. Such highly conducting materials have shown good promise for high energy density batteries. The conductivity behaviour of composites cannot be explained by classical concepts such as doping since the second phase particles are insoluble in the first phase[15].The enhancement in conductivity was found possible by assuming that a highly conducting layer of a few Angstroms thickness surrounds each insulating particle[16].

1.4. General Theory Of Ionic Conductors :

The electrical conductivity of any material is given by,

$$\sigma = \Sigma_i n_i q_i \mu_i \qquad (1.1)$$

where n_i, q_i and μ_i are the concentration, the charge and the mobility respectively of the 'i'th species. The summation is over all possible charge carriers (e.g. vacancies, interstitials, electrons and holes). In most ionic solids the contributions of the holes and electrons to the overall conductivity is negligible compared to those of ions. Assuming that only one type of mobile species makes a significant contribution to the observed conductivity, Eq.(1.1) becomes

$$\sigma = n q \mu \qquad (1.2)$$

where $q = ze$ (z is the valency of the mobile ion and e is the electronic charge).

In poor and moderate conductors the charge carriers are thermally induced interstitial ions (Frenkel defects) or vacancies (Schottky defects) in the crystal structure. The equilibrium concentration of either type of defects is given to a good approximation by

$$n = B\, n_o \exp[-G_s / (2\, k\, T)] \qquad (1.3)$$

where G_s is the energy of formation of a defect pair at the temperature T, n_o the concentration of normal lattice site, and B is an entropy factor which depends upon the crystal structure and the type of defect involved[17].

The variation of mobility with temperature for poor and moderate conductors may be expressed as

$$\mu = (A\, a^2\, e\, \nu)/ (k\, T) \exp[-G_m / (k\, T)] \qquad (1.4)$$

where G_m is the free energy of migration of the mobile species through the lattice, ν is the frequency of vibration, a is the jump distance, and A, a factor which accounts for the change in G_m with temperature[17].

Combining Eqs. (1.1),(1.2) and (1.3) one obtains a general expression for conductivity as follows

$$\sigma = (C / T) \exp [(-G_s / 2 - G_m) / (kT)] \qquad (1.5)$$

In terms of the corresponding enthalpy (H) and entropy (S),

$$G_s = H_s - TS_s \qquad (1.6)$$

$$G_m = H_m - TS_m \qquad (1.7)$$

Eqn. (1.5) can be rewritten as

$$\sigma = (\sigma_o / T) \exp [(-H_s / 2 - H_m) / (kT)] \qquad (1.8)$$

or,
$$\sigma T = \sigma_o \exp [-E_a^{'} / (kT)] \qquad (1.9)$$

where E_a' is the overall activation energy for conduction. Thus a plot of log(σT) vs. 1/T is linear whose slope yields the overall activation energy E_a'. However, since the variation of log T over the experimental temperature range (400K to 750K) is negligible in comparison to that of log σ, a plot of log σ vs. 1/T is also found to be linear and is preferred because of its obvious simplicity. However, the activation energy E_a obtained from this plot is slightly lower than E_a' obtained from Eqn.(1.9) by an amount equal to the thermal energy (kT), i.e. $E_a = E_a' - kT$.

Generally a plot of log σ vs. 1/T for a nominally pure ionic solid consists of two linear segments; a high temperature linear region which is an intrinsic property of the material, and a low temperature extrinsic region characterised by a lower slope (hence lower activation energy). The intrinsic region relates to the temperature range in which the dominant defects are those which are present due to thermodynamic considerations. In this case E_a is the sum of half the formation energy (H_f) and energy of migration (H_m) of defects. The extrinsic region relates to the temperature range in which dominant defects are those introduced by the addition of aliovalent impurities and are present due to charge neutrality conditions. Here E_a is simply the migration energy (H_m) alone. The position of extrinsic - intrinsic transition temperature is known as knee temperature, and is often used as a measure of the impurity level in the crystal. The complete conductivity curve is, therefore, generally a superposition of two line segments corresponding to :

1. $A_1 \exp[-E_1 / (kT)]$ in the low temperature, extrinsic region.
2. $A_2 \exp[-E_2 / (kT)]$ in the high temperature, intrinsic region.

The activation energy E_1 is less than E_2 and A_1 is by far less than A_2. A_2 is independent of the purity of the material, while A_1 increases as the impurity concentration increases in the sample.

1.5. Theory Of Composite Solid Electrolytes :

The enhancement in conductivity of ionic conductor due to dispersion of fine particles of insulators like Al_2O_3, SiO_2 etc. contradicts Maxwell's theory[18] , according to which the conductivity should decrease monotonically with the addition of insulating particles. This phenomenon proclaims that such dispersions are not just simple dilutants. A number of theories have been proposed to explain this curious behaviour of ionic conductors.

1.5.1. Jow and Wagner' s Theory[19] :

Jow and Wagner assumed that the spatial redistribution of defects is the dominant operative mechanism which arises due to some process of charge transfer or interfacial point defect trapping. Two alternative mechanisms were put forth. One is that the formation of a charged double layer, while occurring at or near the dispersions surface, influences the conductivity predominantly via changes in the defect concentration far from each inclusion. The other one is that the major effect on the overall conductivity resides in the much greater enhancement in defect concentration in the double layer itself. The latter possibility was considered more likely since it was able to reproduce certain experimentally observed facts.

If there is a chemically inert phase in contact with a crystal, the space charge profiles can be obtained in a similar way as for a crystal in contact with vacuum. Jow and Wagner treated the problem of conductivity enhancement in CuCl - Al_2O_3 composite system by assuming the existence of a high conducting space charge region at the matrix - particle interface. If the space charge layer around the Al_2O_3 particles is responsible for the conductivity enhancement, then to explain the relation between conductivity, size and volume fraction of the alumina particles, Jow and Wagner considered the conduction in a volume of $(4 / 3)\ \pi\ r_2^3$ containing one single dispersed alumina particle of radius r_1 ($r_2 > r_1$) and expressed the conductivity of the composite σ as follows :

$$\sigma = \sigma_o + \Delta\sigma \qquad (1.10)$$

where σ = ionic conductivity of the bulk

$\Delta\sigma$ = extra conduction due to space charge layer

They assumed that the thickness of the space charge layer λ is smaller than the radius of alumina particle i. e. $\lambda << r_1$ and the excess defect concentration near the surface can be represented by an average excess charge density $<\Delta n_i>$. Then, on simplification $\Delta\sigma$ was expressed as :

$$\Delta\sigma = \Sigma_I\ e\ \mu_I <\Delta n_i> 4\pi r_1^2 \lambda / [(4/3)\ \pi(r_2^3 - r_1^3)] \qquad (1.11)$$

$$\Delta\sigma = 3\Sigma_I\ e\mu_i <\Delta n_i> (r_1/r_2)^3 [\ 1 - (r_1/r_2)^3\ ] \qquad (1.12)$$

where μ_I = mobility of the i^{th} defect species which is assumed to be independent of position. The ratio of r_1/r_2 is a function of volume fraction of the dispersed second phase.

It was further assumed that $r_2 >> r_1$. Then $(r_1/r_2)^3 \approx v_v$, the volume fraction of dispersed phase and the above equation can be rewritten as

$$\sigma = 3\Sigma_I\ e\mu_i <\Delta n_i> \lambda (1/r_1) [\ v_v / (1 - v_v)] \qquad (1.13)$$

where $r_2 >> r_1$ and μ_I , $<\Delta n_i>$ and λ are functions of temperature.

The model provides a qualitative explanation for the conductivity behaviour of composite solid electrolytes. However the model fails to explain the observed maximum in the conductivity at a particular concentration of the dispersion and also the mechanism leading to the enrichment of the defect concentration in the space charge region of various composite solid electrolytes.

Maier[20] treated the space charge region as a separate phase and considered the normally conducting, insulating and space charge layer as a network of parallel resistors. He explained how exactly the surface charge layer is formed on account of possible surface interactions of the mobile defects in the matrix phase with the dispersed second phase allowing a complete and quantitative description of the effect.

The expression for conductivity as derived by Maier is given below

$$\sigma / \sigma_o = (1 - \varphi_A) + K / r_A \qquad (1.14)$$

where

$$K = 3e\sigma_o\beta_L(2\lambda)\varphi_A\mu_v (N_{vo}N_{v\infty})^{1/2}$$

φ_A - volume fraction of insulating phase, σ_o - Conductivity of pure ionic solid, β_L - Correction factor which depends on the topology of insulating phase, λ - Thickness of space charge layer, r_A - size of insulating particle, μ_V - mobility of point defect, $N_{v\infty}$ - concentration of defects in bulk, N_{vo} - concentration of defects in space charge layer

The problem of overall conductivity of dispersed system is very complex. Eqn. (1.14) fulfills the observations made for a variety of composite systems reported in the literature. It explains the linear dependence of σ with φ_A in the low concentration region. For higher volume fractions the blocking effect of alumina becomes important.

1.5.2. Random Resistor Network Model :

This model was proposed by Dietrich and coworkers[21]. It is able to successfully explain the enhancement in conductivity of composite solid electrolytes.

It is assumed that three type of regions exist in the composite material :

a) insulating resistors representing the lack of conduction through the insulating particles.

b) highly conducting resistors representing the enhanced interfacial conductivity.

c) normally conducting resistors representing the conduction in the pure ionic conductor.

Thus, one has the a) and b) type of resistors in a matrix of normally conducting resistors. This is then mapped onto the problem of a random walk on a lattice with three types of bonds, and the diffusion constant is calculated by means of Monte Carlo simulations. The results of the simulations show that the enhanced conductivity starts at a critical concentration of the dispersed particles corresponding to the onset of percolation of highly conducting bonds. However, as the concentration increases, one encounters the second critical concentration where the conducting bonds start forming closed loops inside the system and the conductivity drops drastically leading to the conductor - insulator transition.

1.6. Scope of the present investigation :

Since the effect was discovered in 1973 by Liang[7] , considerable work has been done in the field of composite solid electrolytes. The aim of the present work was

1) to analyse the CsBr-Al_2O_3 composite system with a view to contribute towards a better overall understanding of the conductivity behaviour of composite solid electrolytes

and

2) to test the space charge model for explaining the enhancement in conductivity.

CsBr has been chosen because, barring lithium based compounds, not much work has been done on alkali halides in this particular area of research. Also, CsBr does not undergo any solid-solid phase transformation, its not very hygroscopic and its conduction mechanisms are reasonably well understood.

CHAPTER 2

CHARACTERIZATION TECHNIQUES

2.1. Complex Impedance Spectroscopy :

Theory of Complex Impedance Analysis :

Complex Impedance Spectroscopy is a technique which separates the contribution from various processes such a electrode / electrolyte interface and the migration of charge carrying species through the grains and across grain boundaries. This method was first applied to solid electrolytes by Baurle[22].

The technique involves applying a sinusoidal signal of low amplitude across the sample kept between two electrodes. The output signal, which is also a sine wave, is compared with the input signal to determine the impedance modulus and phase shift corresponding to the equivalent circuit which represent the assembly i.e. electrode / electrolyte / electrode. The complex impedance $Z(\omega)$ at an applied frequency ω can be written as :

$$Z(\omega) = Z_R(\omega) + jZ_I(\omega) \qquad (2.1)$$

where Z_R is the real and Z_I is the imaginary part of the complex impedance. The magnitude of the complex impedance is

$$Z = (Z_R^2 + Z_I^2)^{1/2}$$

and the phase angle is

$$\theta = \tan^{-1}(Z_I / Z_R).$$

This can be represented vectorially as shown in fig. 2.1. For a resistance R and a capacitance C in parallel, the complex impedance is given by :

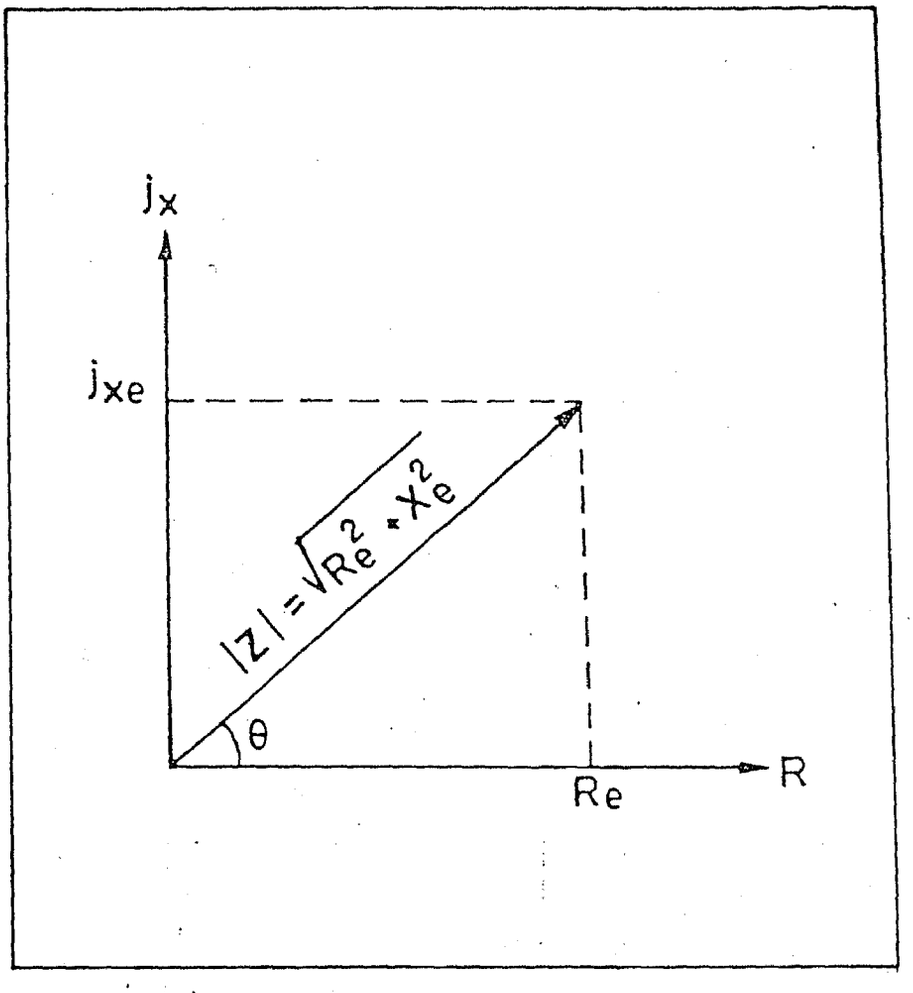

FIG 2.1. IMPEDANCE VECTOR REPRESENTATION

$$Z(\omega) = \frac{R[1 / (j\omega C)]}{[R + 1/(j\omega C)]} \qquad (2.2)$$

or

$$Z(\omega) = \frac{R}{(1 + \omega^2 C^2 R^2)} + j\frac{-R^2\omega C}{(1 + \omega^2 C^2 R^2)} \qquad (2.3)$$

Thus the real and imaginary parts of $Z(\omega)$ are :

$$Z_R = \frac{R}{(1 + \omega^2 C^2 R^2)} \qquad (2.4)$$

$$Z_I = \frac{-R^2\omega C}{(1 + \omega^2 C^2 R^2)} \qquad (2.5)$$

Elimination of ω from (1.15) and (1.16) yields :

$$(Z_R - R/2)^2 + Z_I^2 = R^2 / 4 \qquad (2.6)$$

which is the equation of a circle of radius R/2, with its centre at (R/2 , 0).

Fig. 2.2 shows the complex impedance plots for pure resistors and capacitors separately. Fig. 2.3 shows the impedance plot for different combinations of resistors and capacitors. The simplest equivalent circuit representation of the system is shown in Fig. (2.3. a). This is true only if non-blocking electrodes are used. The equivalent circuit for a system with blocking electrodes is depicted in Fig (2.3.b). C_{dl} here represents the capacitance at the electrode / electrolyte interface. In this case, apart from the semi-circle, a 90° line is also obtained for perfectly smooth surfaces. The slope of this line decreases as the surface roughness increases[23].

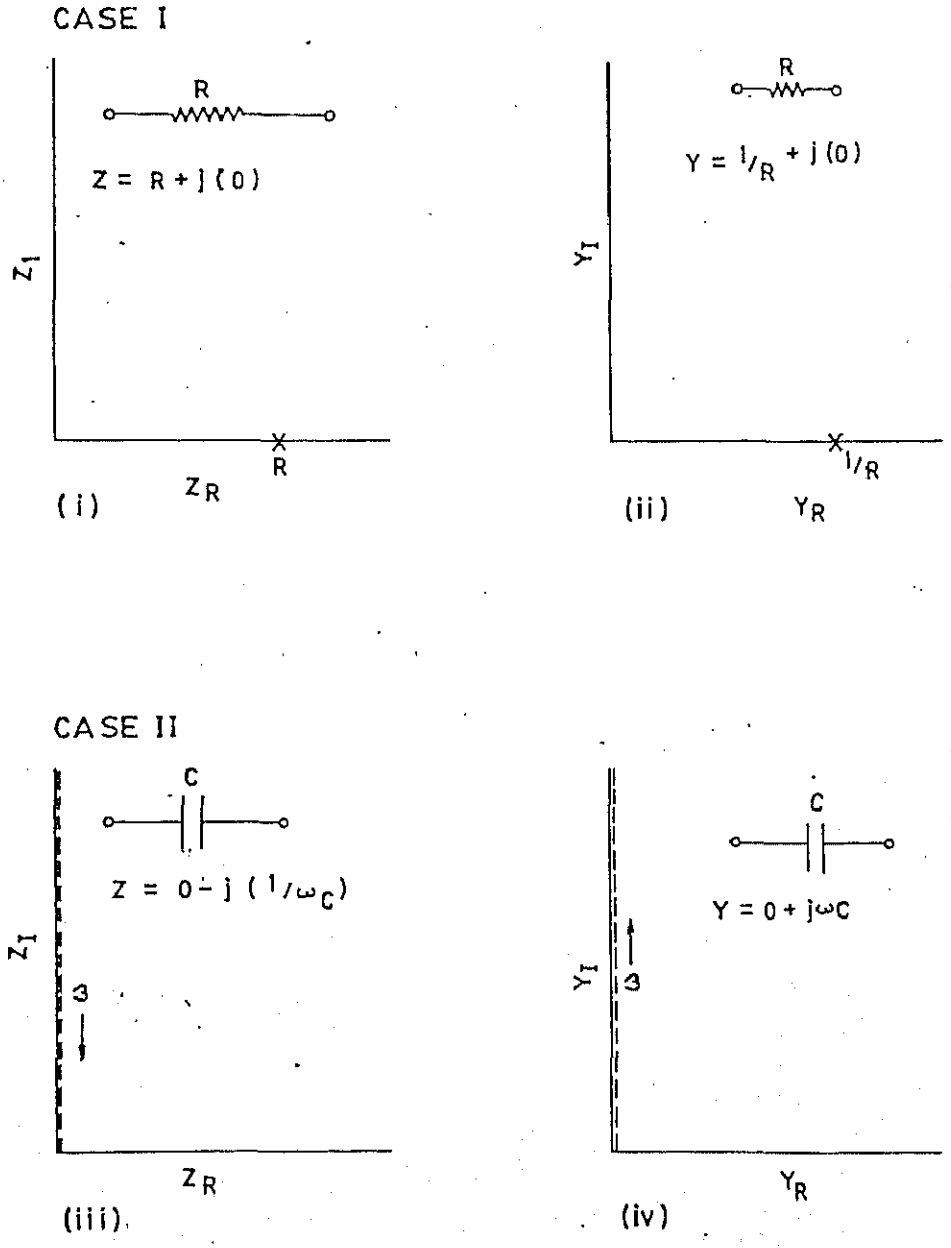

FIG. 2.2. COMPLEX IMPEDANCE PLOTS

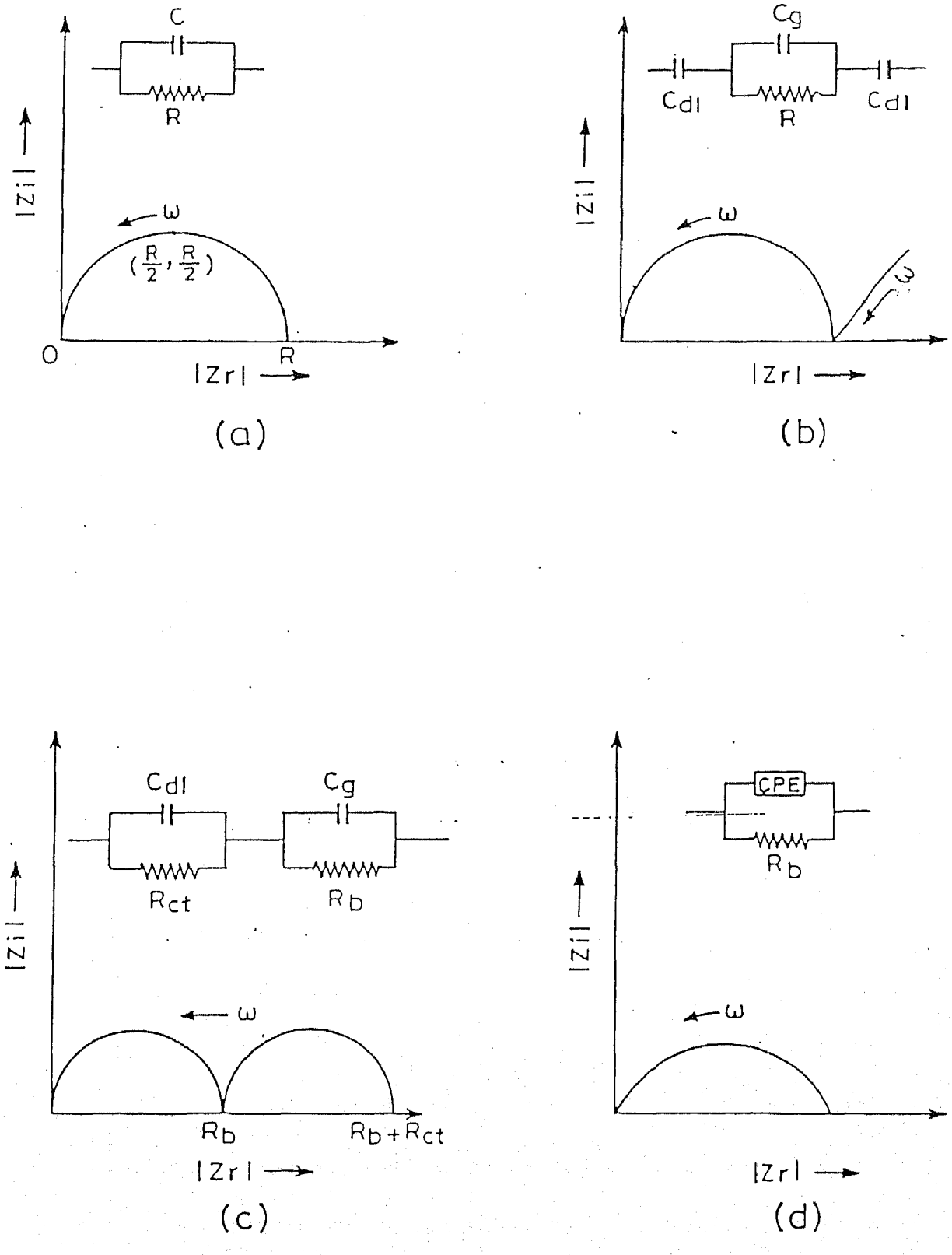

Fig.2.3. Various impedance behaviours observed in solid electrolytes.

For a polycrystalline material there may be some contribution to the conductivity from the grain boundaries. In some of these cases one may detect a second semi-circle in the impedance plot (Fig 2.3.c)[23,24]. The bulk resistance in such cases is obtained from the intersection of the semi-circle with the real axis in the low frequency region. A study of the conductivity dependence on grain size may help to identify the mechanism of conduction.

Another common impedance behaviour is one in which the semi-circle is depressed so that the centre is situated below the real axis (Fig 2.3.d). This type of frequency response can be represented by a constant phase element[25,26]. The complex admittance of the CPE is given by :

$$Y = Y_o (j\omega)^n \qquad (2.7)$$

or

$$Y = Y_o \omega^n e^{jn\pi/2} \qquad (2.8)$$

$$Y = Y_o \omega^n [\cos(n\pi/2) + j\sin(n\pi/2)] \qquad (2.9)$$

where n is a constant. If $n = 0$, the constant phase element represents a pure resistor with $R = 1 / Y_o$. If $n = 1$, the CPE represents a pure capacitor, $C = Y_o$ and if $n = -1$, it is a pure inductor with $L = 1 / Y_o$.

The two main advantages of impedance spectroscopy are :

(I) It involves relatively simple electrical measurements that can be readily automated and (II) The results can often be correlated with material variables such a composition, microstructure, defects, dielectric properties, chemical reactions etc. A detailed analysis of the impedance data in terms of appropriate model of the electrode - electrolyte system can also provide one with many other vital microscopic parameters such as mobility, electrode reaction, rate constant etc. This also characterises the interface and bulk properties of the undertaken system. In case of polycrystalline materials a proper analysis may lead to

valuable information about the inter-grain and intra-grain properties. It can also predict the performance of a device such as chemical sensors and fuel cells.

The disadvantage of the method, however, is the difficulty to determine unambiguously the appropriate equivalent circuits and to estimate the values of the critical parameters. In order to distinguish between external equivalent circuits some knowledge is required of chemical and physical processes involved.

2.2. Experimental Details :

2.2.1. Sample Preparation :

CsBr (99.9% purity) was obtained from Aldrich Chemicals Inc. USA.

Physical Properties :

Molecular weight : 212.81g

Bravais lattice : Simple Cubic

Density : 4.440 g/cc

Melting Point : 636 ° C

Boiling Point : 1300 ° C

Al_2O_3 was obtained from Buehler Micropolish II, USA.

Physical Properties :

Molecular weight : 101.96 g

Bravais lattice : fcc (γ - Al_2O_3), rhombohedral (α - Al_2O_3)

Density : 3.5-3.9 g/cc (γ - Al_2O_3), 3.97 g/cc (α - Al_2O_3)

Melting Point : 2015 ± 15 ° C

Boiling point : 2980 ± 60 ° C

Table 2.1.

Details Of Preparation Of Samples

Composition	Weight		Pelletization Pressure ton / cm^2	Temperature and duration of heating for homogenisation	
	CsBr (gm.)	Al_2O_3 (gm.)		temp ($^\circ$ C)	time (hrs.)
CsBr	2.00	0.00	6	500	10
CsBr - 10 m / o Al_2O_3	1.89	0.10	6	500	10
CsBr - 20 m / o Al_2O_3	1.74	0.26	6	500	10
CsBr - 30 m / o Al_2O_3	1.66	0.35	6	500	10
CsBr - 35 m / o Al_2O_3	1.59	0.41	6	500	10
CsBr - 40 m / o Al_2O_3	1.51	0.49	6	500	10
CsBr - 50 m / o Al_2O_3	1.35	0.65	6	500	10

Dried powders of CsBr and alumina were taken in the proper proportions and mixed thoroughly in an agate mortar and pestle. Table 2.1. gives the details of sample quantities required for various compositions. The grinding resulted in a very fine-powdered composite. This fine powder was transferred to a stainless - steel die which was placed in a hand - operated hydraulic press. The die was thoroughly cleaned with acetone before use. A pressure of 6 tons / cm^2 was applied on the die. The diameter of the pellets was fixed by the diameter of the die piston which was 12 mm. The thickness of the pellets ranged from 3 to 4 mm. The pellets were sintered at about 100 $^{\circ}$ C below the melting point of CsBr and stored in small specimen bottles. The density of the sintered pellets was calculated by measuring their dimensions and masses. The density was found to be around 90 % of theoretical density for all the samples.

2.2.2. Sample holder :

Fig 2.4 shows the schematic diagram of the sample holder. It consisted of three identical lava discs (diameter ~ 2.5 cm and thickness ~ 1 cm), each having a central hole and four symmetrically located holes near the periphery. The lava discs, after machining were heated slowly to 1000 $^{\circ}$ C and kept at that temperature for two hours before cooling inside the furnace. This kind of heat treatment was necessary to harden the lava disc and also to remove any moisture content. The effect of the latter was to increase the resistivity of the disc significantly. A pair of stainless steel rods were passed through the two diametrically opposite holes to provide support to the sample holder. The spring which was so located that it remains outside the furnace, applied uniform pressure due to spring action to ensure a firm contact between the electrodes and the sample. A quartz tube was used to provide the body of the sample holder.

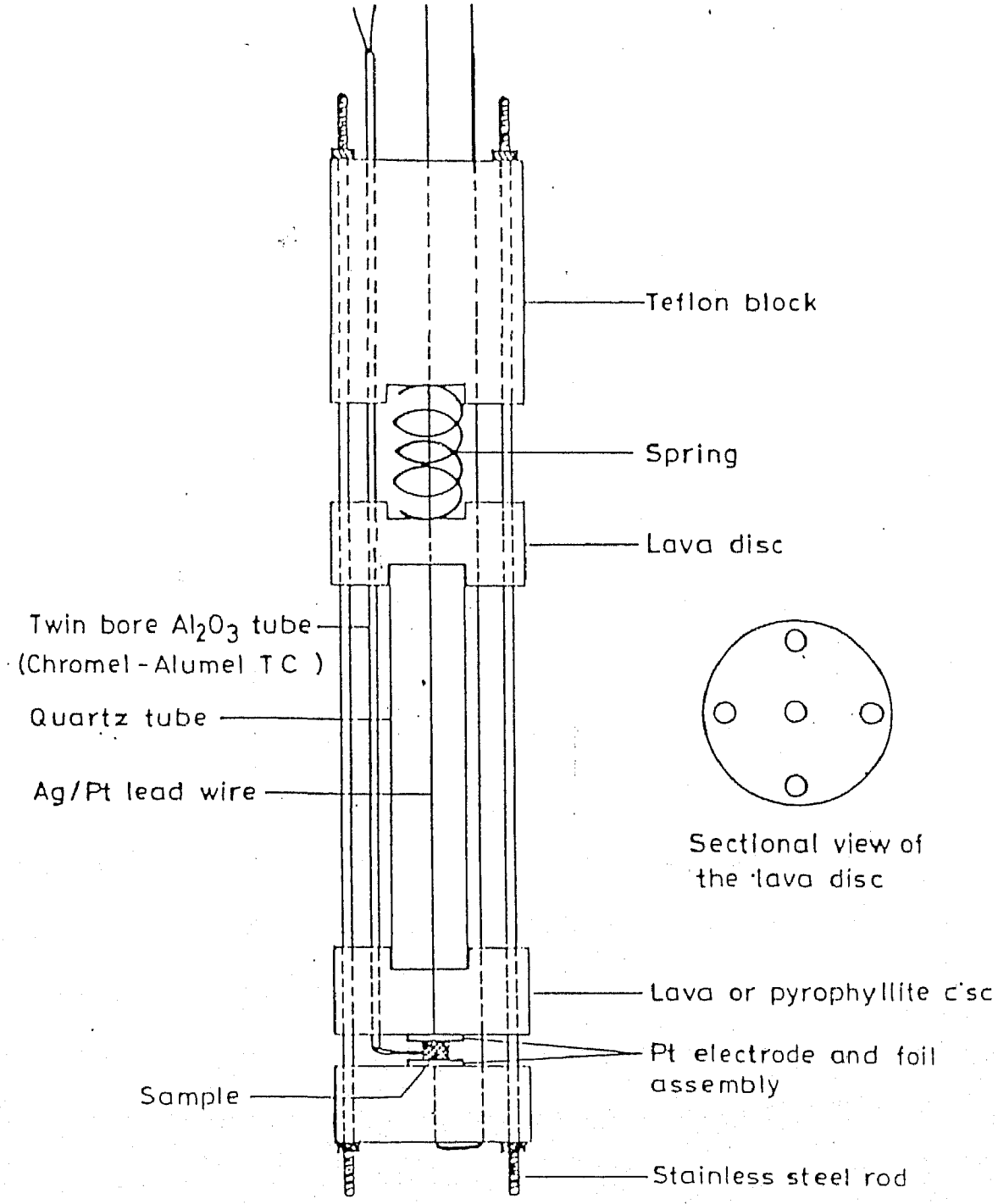

FIG 2.4 SAMPLE HOLDER FOR ELECTRICAL CONDUCTIVITY MEASUREMENTS FROM ROOM TEMP. TO 1000° C

The flat surfaces of the cylindrical pellets were polished on different grades of fine polishing papers to remove the surface contamination and to obtain smooth and parallel surfaces. The pellet was carefully placed between the two platinum electrodes. The spring mechanism ensured that there was a firm contact between the electrodes and sample .

2.2.3. Furnace and temperature controller :

An electrical resistance heating furnace comprising of a mullite tube (diameter ~ 1.5 inches) over which kanthol wire of 22 gauge was wound inductively and uniformly has been used. The resistance of the heating element was ~ 43 Ω. A high temperature cement was applied over the kanthol winding to fix them in place. The mullite tube with cemented kanthol wiring was enveloped with a cylindrical stainless steel container, and the space between the two shells was filled with MgO powder to minimise the heat loss.

The temperature inside the furnace was measured using a chromel - alumel thermocouple. Care was taken to ensure that the sample and the hot junction of the thermocouple were as close to each other as possible since the temperature throughout the furnace will not be uniform.

A PID type temperature controller (Indotherm, Model 401D) was used to control the furnace temperature. The temperature was controlled to within $\pm 1^{\circ}C$.

2.2.4. Impedance Analyser :

Fig. (2.5) shows the block diagram of the impedance measurement set - up. HP 4192A Impedance Analyser along with HP 16047A test fixture has been employed for the

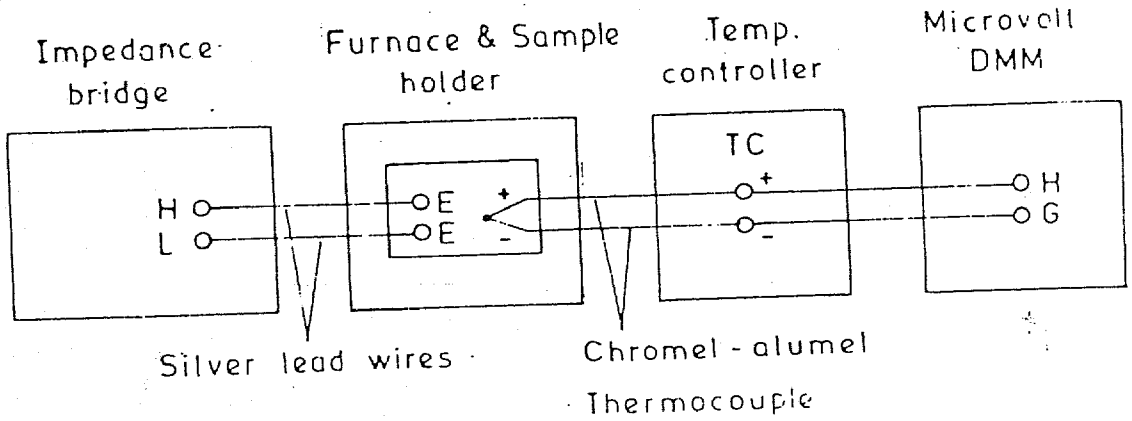

FIG 2.5 Block diagram connections for electrical conductivity measurements

complex impedance measurements. The equipment was an auto balancing bridge with a test signal from 5 mV to 1.1 V with 1 mV resolution. It had a built - in frequency synthesizer which has a frequency range 50 Hz to 13 MHz with 1 mHz frequency resolution. There were two display sections, namely Display A and Display B, which provided direct readout of the selected measurement parameters.

For connecting the sample to be tested, the HP - 4192A employed measurement terminals in a four terminal pair configuration which had a significant measuring advantage for component parameter requiring high accuracy in the high frequency region. Generally, any mutual inductance, interference of the measurement signals, and unwanted residual factors in the connection method which were incidental to ordinary terminal methods significantly affect the measurement at a high frequency. The four terminal pair configuration measurement permitted easy, stable and accurate measurements and avoids the measurement limitations inherent in such effects. Fig. 2.6 shows the four terminal pair measurement principle. The unknown terminals consist of four connectors : High current (H_{cur}), High potential (H_{pot}), Low potential (L_{pot}) and Low current (L_{cur}). The purpose of the current terminals is to cause a measurement signal current to flow through the device under test (DUT) or sample. The potential terminals are for detecting the voltage drop across the sample. The high side represents the drive potential with reference to the low side potential drawn from the internal measurement signal source. The main principle is that the measurement signal current does not develop an inductive magnetic field and thus the test leads do not contribute additional measurement errors due to self or mutual inductance between the individual leads. However, the four terminal system must be converted to a two terminal configuration at / near the sample because the sample / device under test (DUT) has two leads.

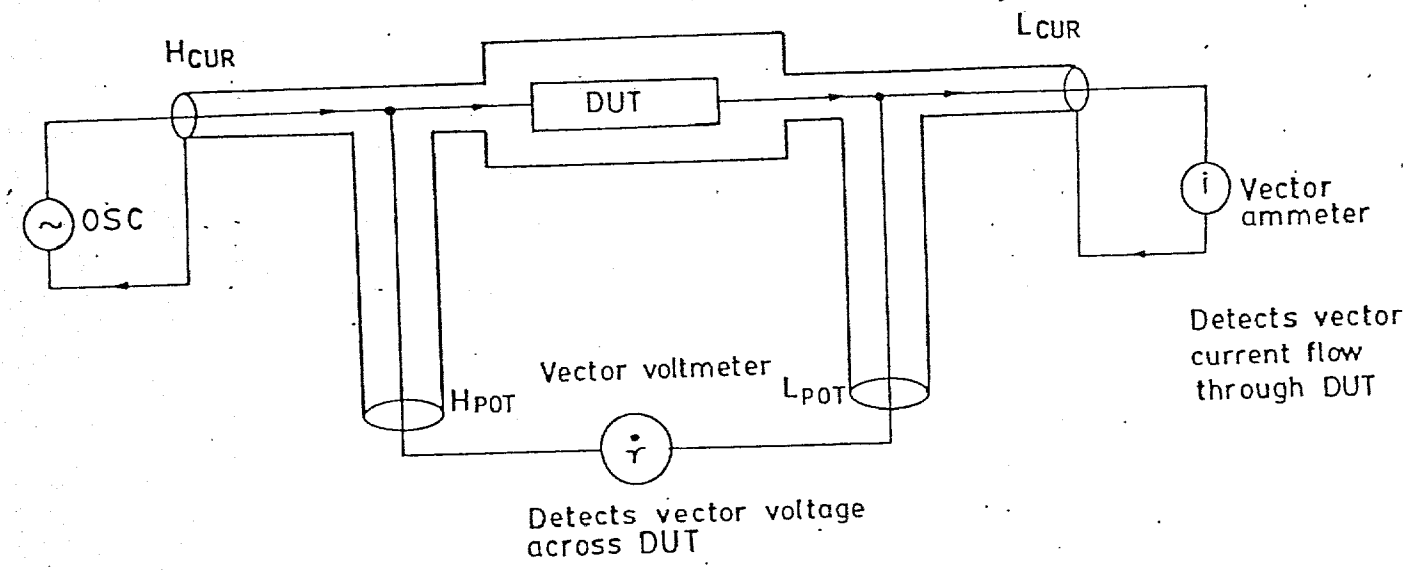

FIG. 2.6. FOUR TERMINAL PAIR MEASUREMENT PRINCIPLE

The impedance measurements were carried out generally in the heating cycle at a temperature interval of around 30 ° C. Sufficient time (30 mins.) was allowed at each temperature for attainment of thermal equilibrium.

2.3. X - Ray Diffraction (XRD) :

X - Ray diffraction patterns of various compositions have been recorded using a Richeifert (Iso - Debyeflex 200 2D) counter diffractometer employing a filtered Cu K_α radiation ($\lambda = 1.542$ Å). The generator was operated at 30 kV and 20 mA. The scanning speed was 3 ° per minute in 2θ . All XRD patterns were recorded at room temperature.

While recording the XRD patterns, it was observed that some of the samples picked up moisture from the atmosphere leading to additional peak attributable to their hydrates. To avoid this problem the powder samples were predried at a sufficiently high temperature to remove water content and were then quickly spread on to a glass slide, followed by spraying Krylon No. 1303 crystal clear acrylic spray coating. The XRD results obtained from these samples were found satisfactory.

2.4. Differential Thermal Analysis :

The Differential Thermal Analysis involves the heating / cooling of the test sample at a constant rate alongwith a reference sample which does not undergo any phase transformation or thermal event in the temperature range of investigation. Any phase change or chemical reaction accompanied by absorption or evolution of heat can be readily detected by DTA. The phase transformation temperature can be determined by this method and hence the presence or absence of the phase can be known.

In order to confirm that alumina does not form any solid solution or a new phase with the matrix material, all the samples have been investigated by DTA. A mini DTA equipment (Linseis L62) has been employed to carry out the DTA measurements. The equipment employs a helics-shaped SiC heating element of very small heat capacity which permits a fast and efficient heating / cooling rate over a wide range or temperature (room temperature to 1500 ° C) . Pt / Pt - 13 % Rh thermocouple was used to measure the temperatures of the test (T_{est}) and the reference (T_{ref}) samples and hence the temperature difference $\Delta T = T_{test} - T_{ref}$. The reference junctions of the thermocouple were kept at the bottom of the furnace where a constant temperature was maintained by water circulation.

Platinum rather than alumina crucibles were used to load both reference and the test samples to obtain a better thermal sensitivity. Al_2O_3 powder was invariably used as a reference material. Because of the considerable error involved at large heating / cooling rates, and the poor resolution obtained at slower heating / cooling rates, the heating / cooling rate was optimised at 10 ° C per minute for best result after making several trial runs. The DTA equipment was standardised by means of several high purity materials of known melting points., though it was ultimately concluded that an error of ± 10 ° C was unavoidable in the temperature range of 500 to 800 ° C at a 10 ° C per minute heating / cooling rate.

Since the samples were hygroscopic, they were dried to remove any trace of moisture before the DTA was carried out. This was done to prevent the formation of a small endothermic peak corresponding to the melting point of water.

2.5. Scanning Electron Microscopy :

The SEM studies were carried out using Jeol model JSM - 840A scanning electron microscope to examine the size and the distribution pattern of Al_2O_3 particles in the matrix material. The equipment has a range of magnification from 10x to 30000x. The surface of each sample was polished on very fine emery paper and cleaned with acetone. The micrographs were taken at 10^{-11} A probe current and 15kv accelerating voltage. The magnification was fixed according to the need.

CHAPTER 3

RESULTS AND DISCUSSION

This chapter discusses the conduction characteristics of CsBr - Al_2O_3 composites . It is widely accepted that in composite solid electrolytes, the conductivity enhancement occurs because of increased concentration of defects in the space charge layer adjoining the dispersoid[19,20,27,28]. However, the direct evidence for the existence of space charge layer is still a subject of intensive investigation.

Most of the sample are investigated by DTA, powder XRD and SEM techniques for phase analysis and microstructural characterisation. The dc conductivity of the samples at different temperatures is obtained from complex impedance analysis.

3.1. X - Ray Diffraction :

The X - Ray diffraction(XRD) pattern of all the samples were taken before and after heat treatment and observed for the presence of any new phases. Fig. 3.1. shows the XRD patterns at room temperature of CsBr-30 m/o Al_2O_3 samples. Figs. 3.1.a. and 3.1.b. show the pattern before and after sintering the sample at 500 ° C. It is possible that there may be overlapping of lines of the two different phases. However, it is clear from these results that there are no new peaks or shift in the peaks because of solid-solution formation or because of some solid-state reaction. This is one confirmation that the sample remains a composite.

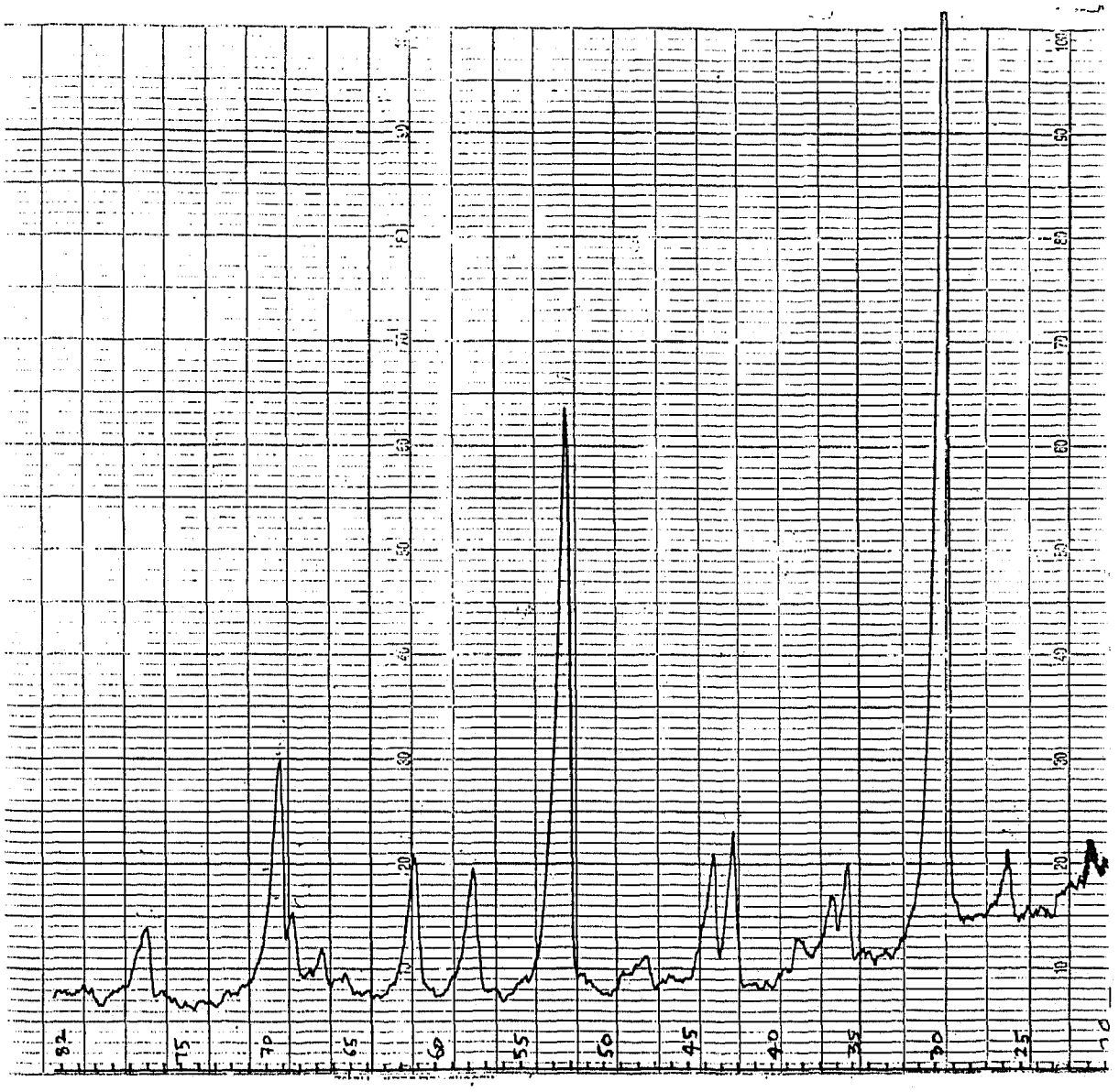

Fig. 3.1 (a) XRD pattern Of CsBr-30 m/o Al_2O_3 before sintering

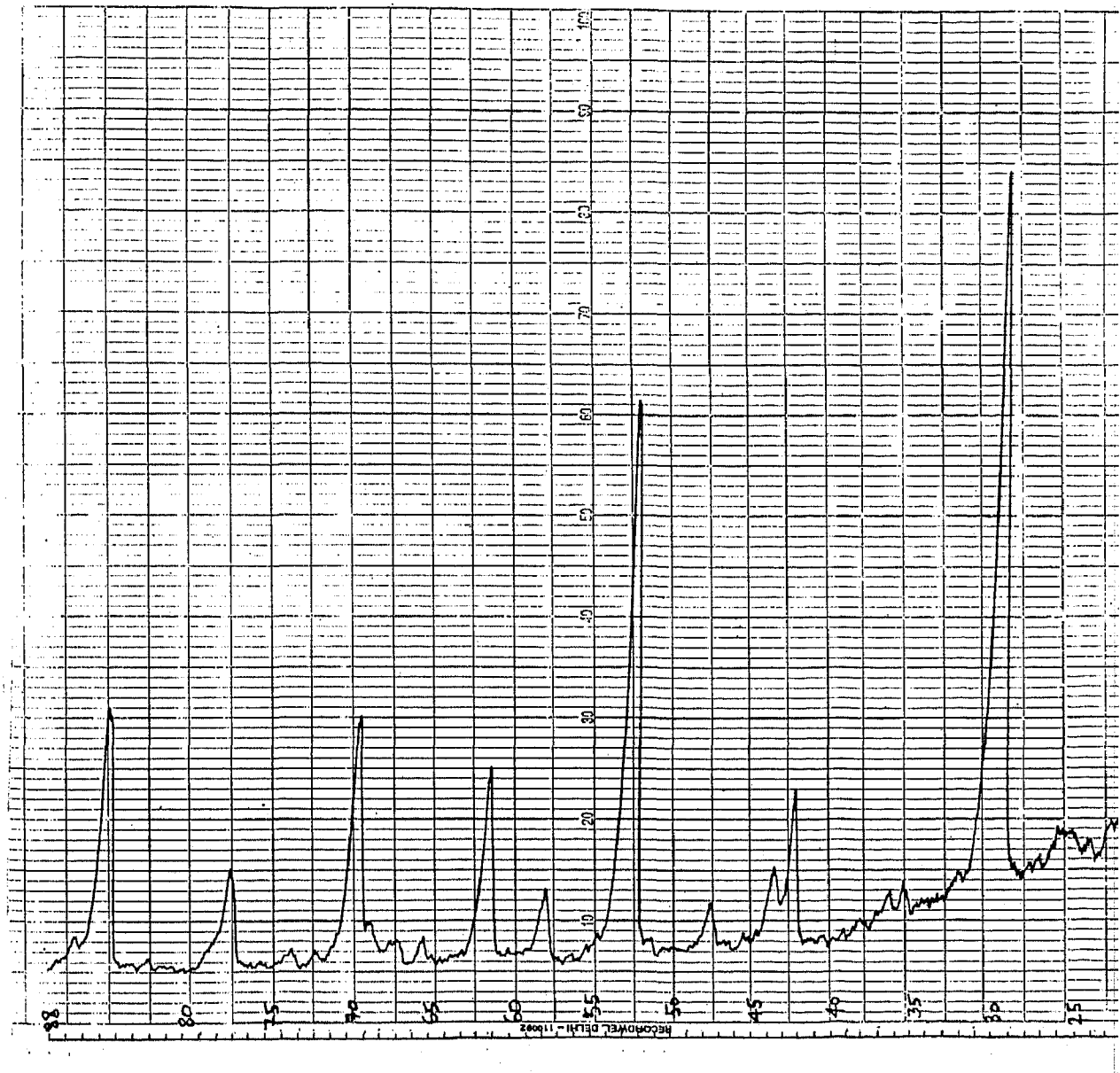

Fig. 3.1 (b) XRD pattern of CsBr-30 m/o Al_2O_3 after sintering at 500 ° C

Since the XRD pattern was taken at room temperature, there is another possibility that some kind of solid state reaction or single phase formation occurred at high temperatures. This is ruled out by subjecting the sample to Differential Thermal Analysis.

3.2. Differential Thermal Analysis :

All the samples were subjected to Differential Thermal Analysis(DTA) for verification of the melting point and to detect if any other thermal event occurred before the melting point. Figs. 3.2. (a), (b) and (c) show the DTA curves for pure CsBr and CsBr-Al_2O_3 composites for two different compositions (10 m/o and 30 m/o). The only thermal event observed in this case being the melting of CsBr which occurs at 636 ° C. The DTA output clearly rules out the formation of any new phase. The peaks of 10 m/o and 30 m/o Al_2O_3 dispersed samples are smaller than that of pure CsBr simply because the amount of CsBr present in these samples is lesser. Also the DTA output of 30 m/o Al_2O_3 sample shows more noise peaks which may be due to local fluctuations in the sample. Thus we can confirm from DTA that Al_2O_3 remains as a separate phase in the sample till the melting point of CsBr is reached.

3.3. Scanning Electron Microscopy:

The scanning electron micrographs for pure CsBr and CsBr-35 m/o Al_2O_3 composite sintered at 500 ° C are shown in Fig.3.3. In case of pure CsBr, the grains are uniformly distributed, whereas in the case of CsBr-35 m/o Al_2O_3 the two phase microstructure of CsBr interspersed with Al_2O_3 is observed.

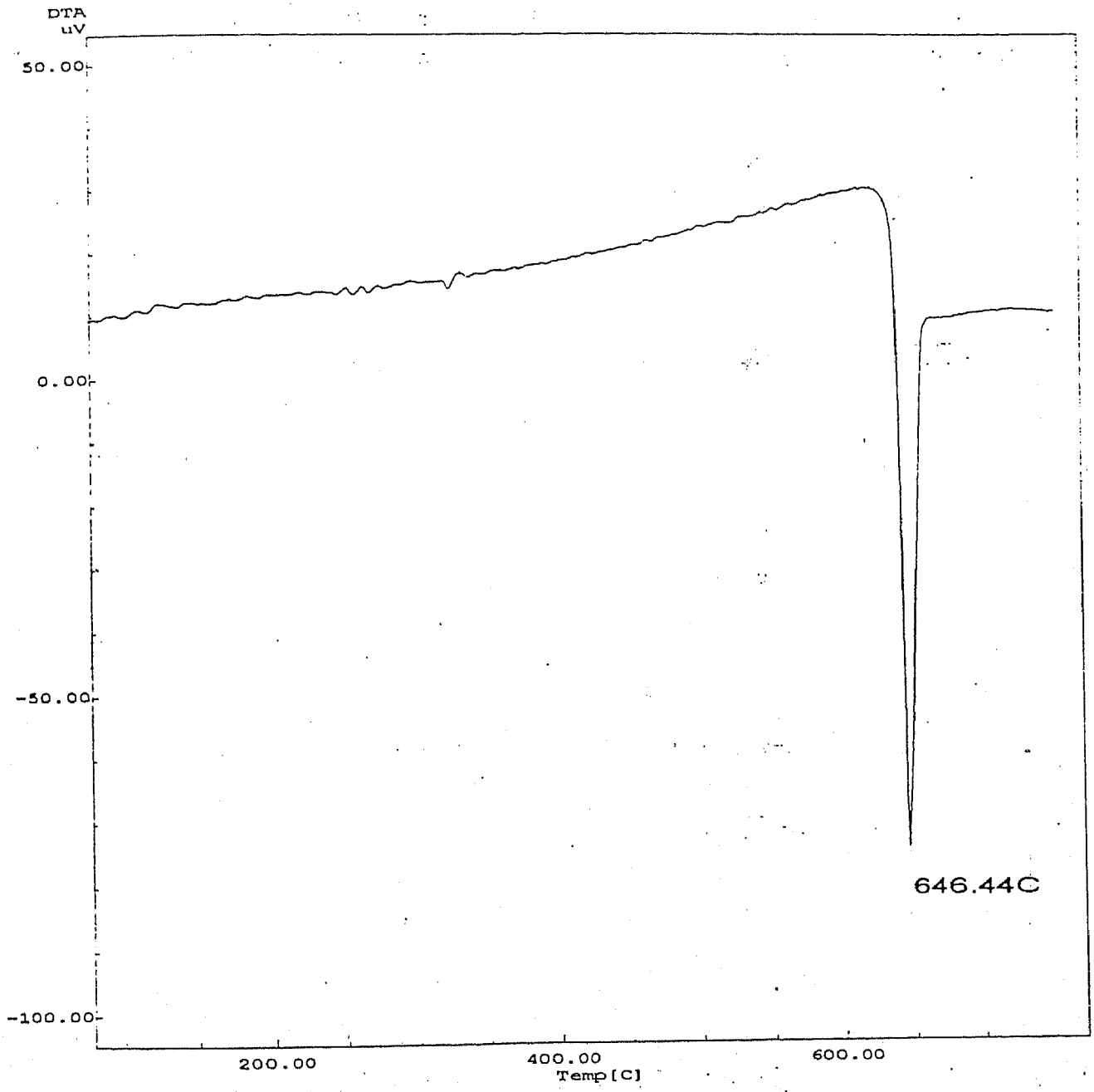

Fig. 3.2 (a) DTA curve for pure CsBr.

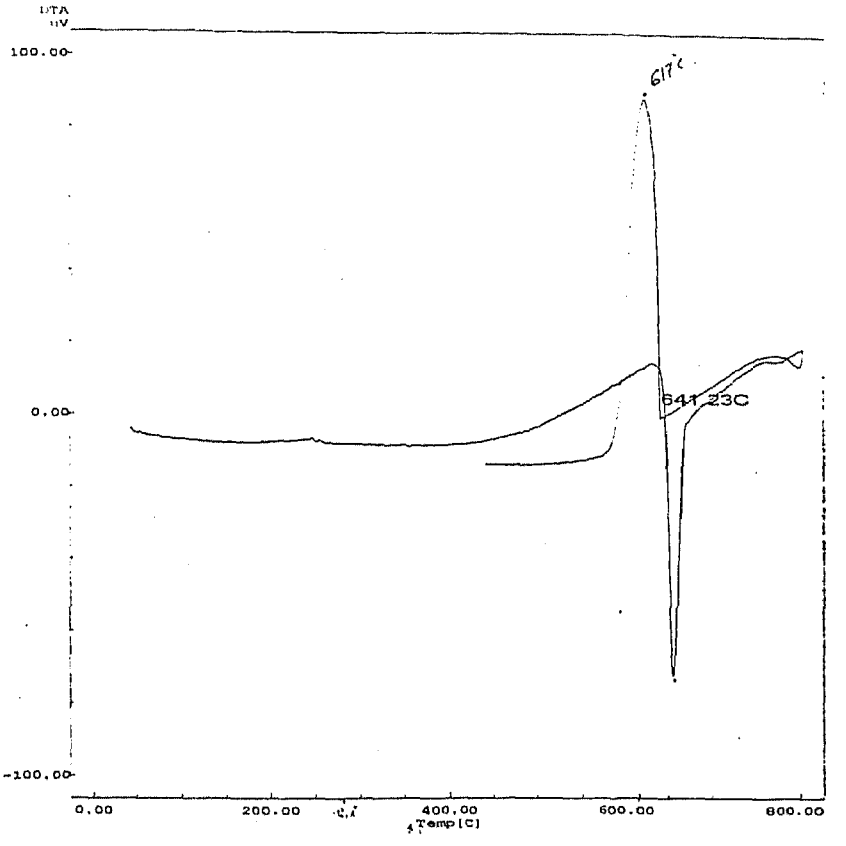

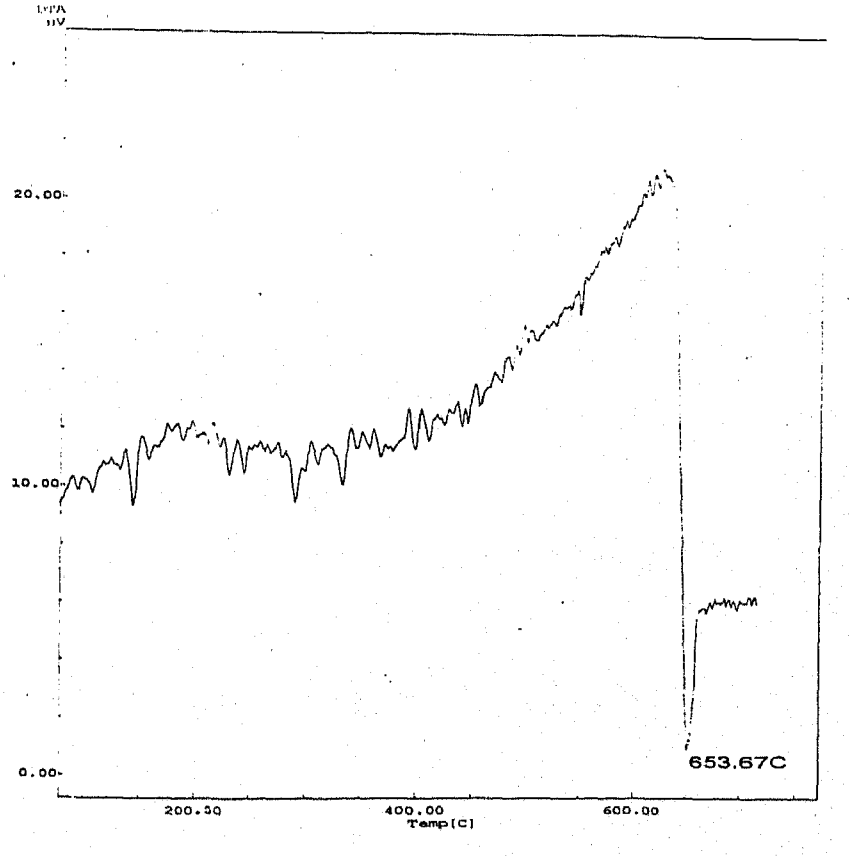

Fig. 3.2 (b) and (c) DTA curves for CsBr - 10 m / o Al_2O_3 and CsBr - 30 m / o Al_2O_3

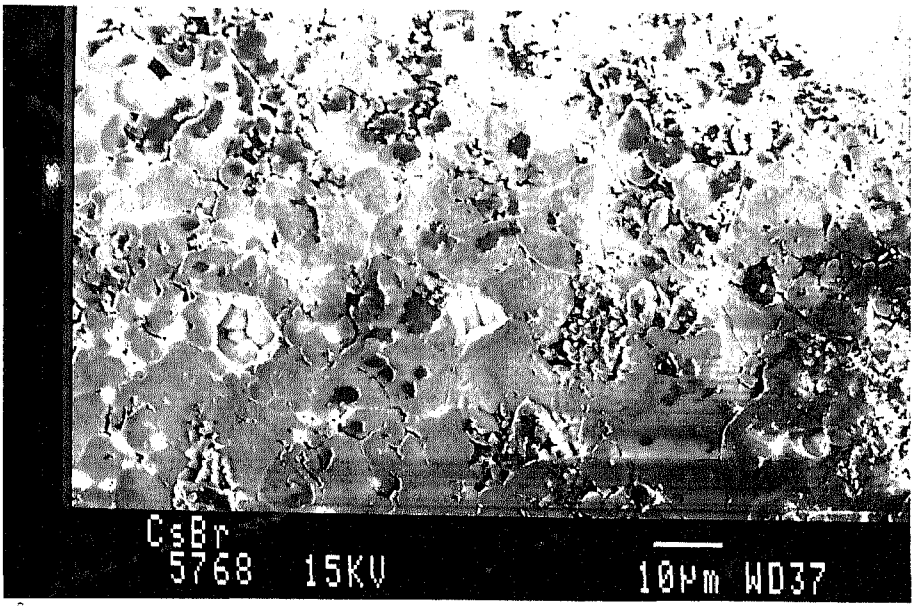

Fig. 3.3 (a)

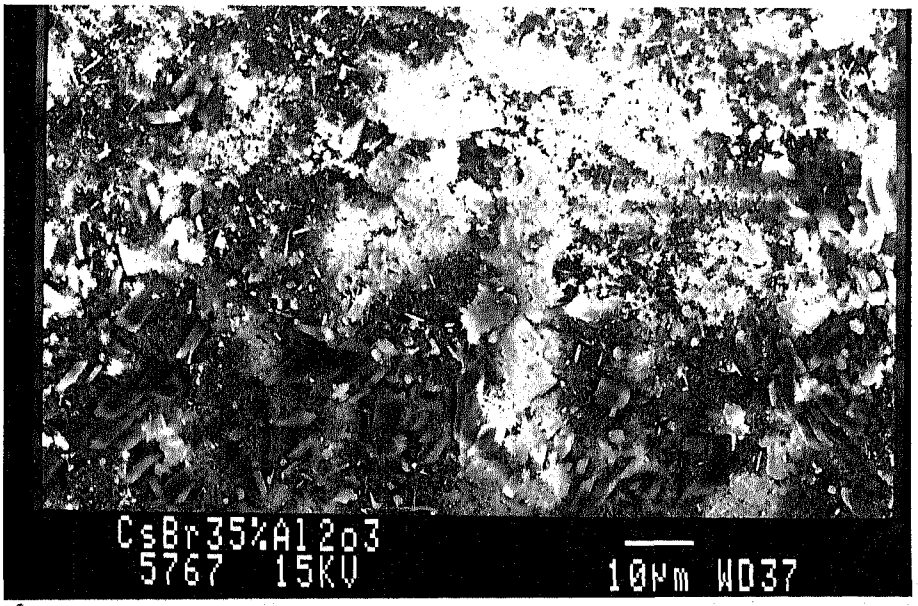

Fig. 3.3 (b)

SEM micrographs of pure CsBr and CsBr-35 m/o Al_2O_3

3.4. Complex Impedance Analysis :

The cell assembly i.e. the sample + electrodes + leads, represents a complex impedance involving resistance and reactance. The reactance arises due to the capacitance between the electrodes and the sample, the capacitance due to grain boundaries etc. Thus the unknown sample is like a black box consisting of resistance and capacitance in an unknown configuration. Hence to determine the resistivity / conductivity of the sample complex impedance analysis has been used.

Figs. 3.4 to 3.6. show the complex impedance plots at different temperatures for different concentrations of alumina. The impedance data (Z and θ) were collected for a range of frequencies from 1 kHz to 4 MHz. An impedance plot is obtained by plotting $Z\cos\theta$ against $Z\sin\theta$. The diameter of each plot gives the dc resistance of the sample under study at one particular temperature. By measuring the geometry of the sample using screw-gauge, the conductivity can be calculated using the following relation

$$\sigma = L / (A * R) \qquad (3.1.)$$

where

L - Length of the sample

A - Area of cross - section of the sample

R - Resistance of the sample

Thus, it is obvious that a large number of data points are needed just to obtain the conductivity at one temperature.

It is seen that the centres of the semi-circles are depressed with the centre not exactly lying on the X - axis. Another characteristic feature of the impedance plot at low

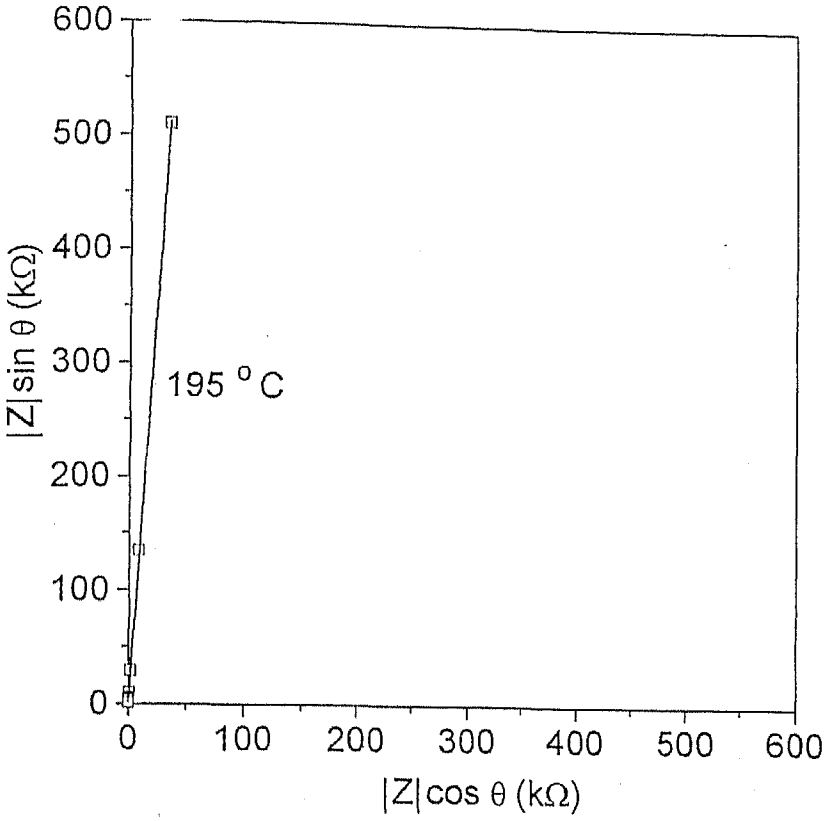

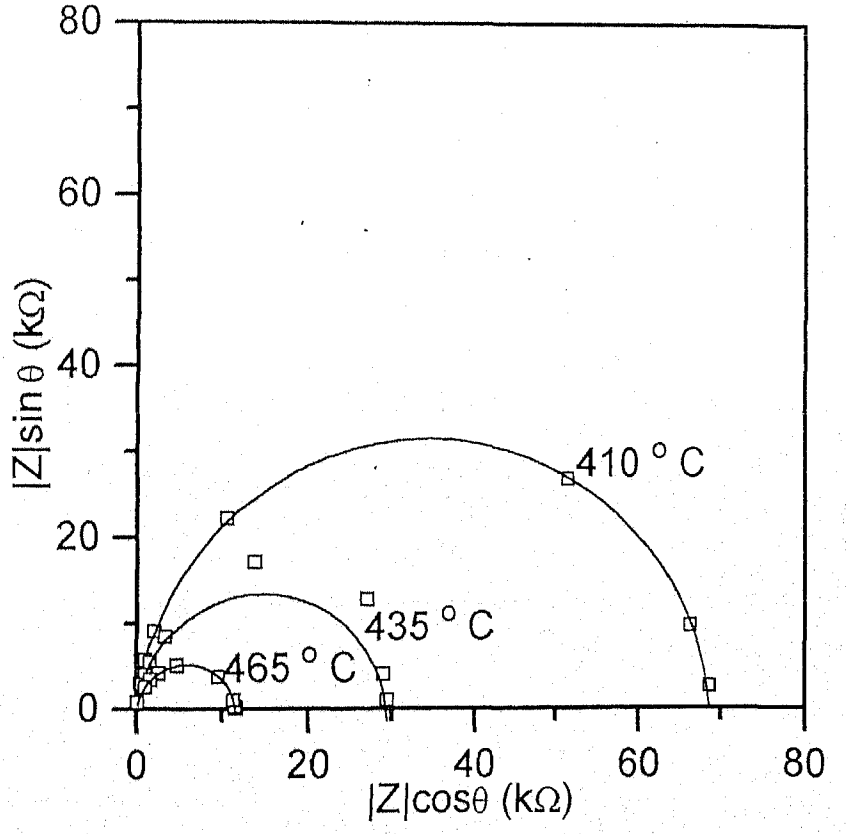

Fig. 3.4. (a), (b) Complex Impedance Plots for pure CsBr.

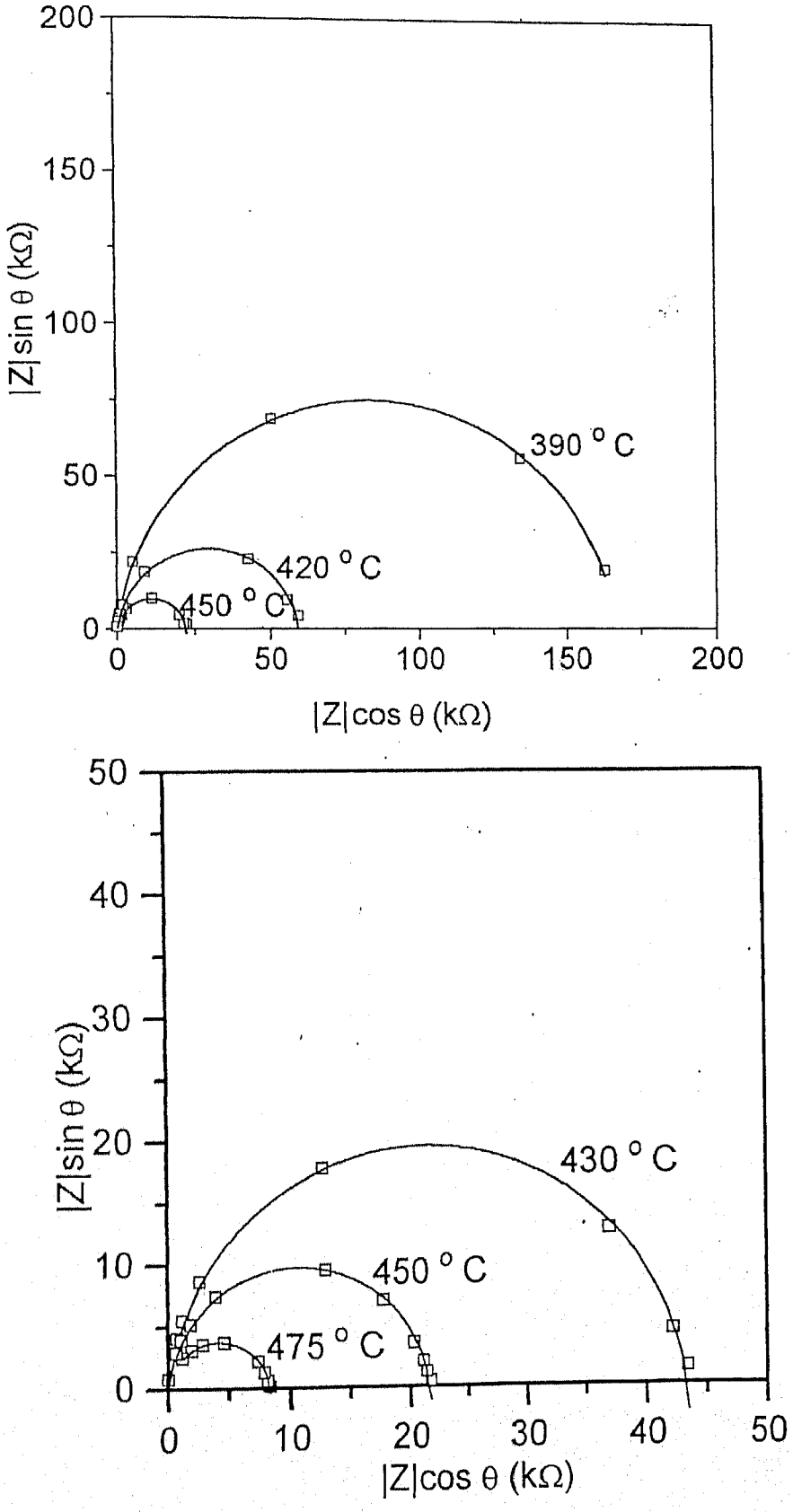

Fig. 3.5. (a), (b) Complex Impedance Plots for CsBr - 10 m / o and 20 m / o Al_2O_3.

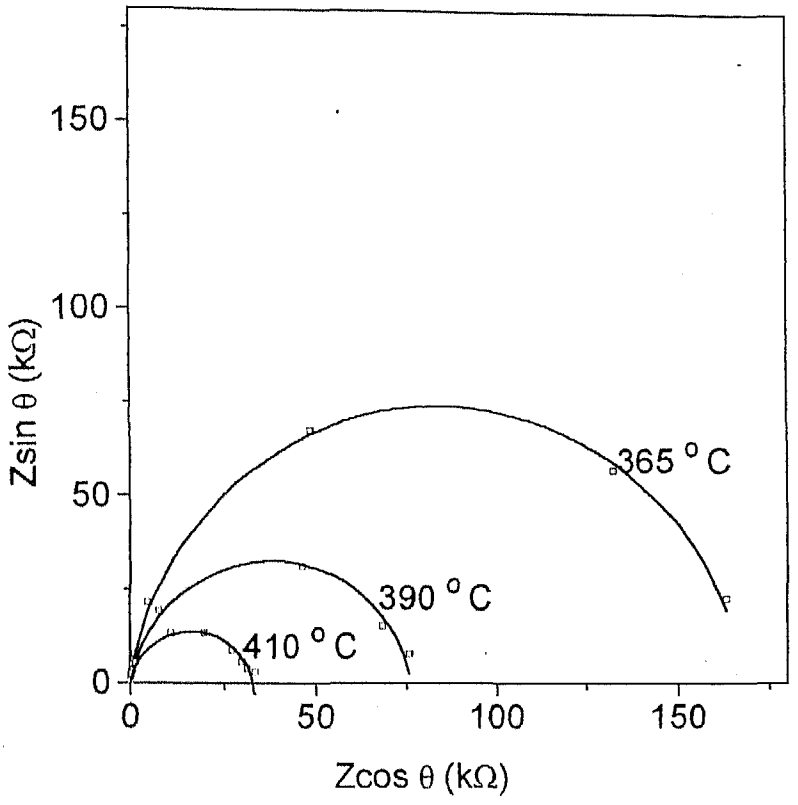

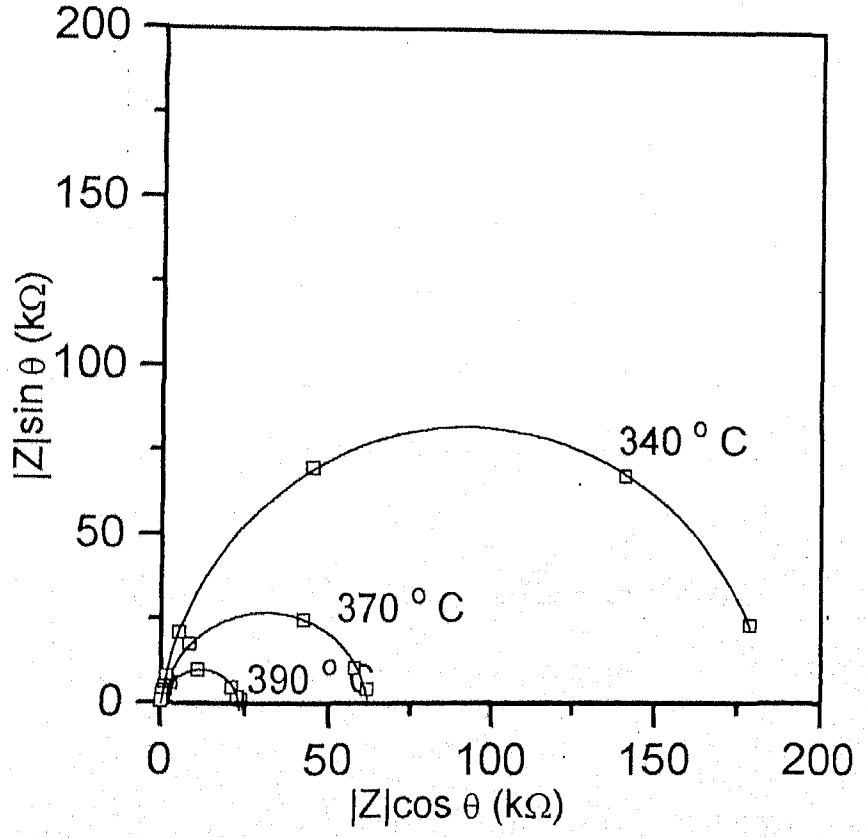

Fig. 3.6. (a), (b) Complex Impedance Plots for CsBr - 30 m / o and 35 m / o Al_2O_3.

temperatures is that the phase angle θ remains constant with frequency. This can be seen in Fig. 3.4 (a). This is not uncommon in impedance spectroscopy because the sample is not just a simple combination of resistor and capacitor. As mentioned in Section 2.1.1. it can be modelled as a parallel combination of a resistor and a constant phase element (CPE) which has an impedance of $Z = A(j2\pi f)^{-n}$, where A is a constant and exponent 'n' has a value between 0 and 1.

The linear impedance behaviour at 195 ° C for pure CsBr can be described as,

$$Z = |Z| (\cos\theta + j\sin\theta) \qquad (3.2.)$$

where $\theta \approx 86$ °. comparison of Eqn. 2.9 with Eqn. 3.2 yields the value of n for the sample.

$$\theta = 86^{o} = n\pi/2$$

or $$n = (2/\pi)(86x\pi/180) \approx 0.95.$$

As discussed in Section 2.1.1 a CPE with n = 1 represents a pure capacitor. Thus n = 0.95 suggests that the behaviour of our sample - electrode assembly at lower temperatures approaches that of a pure capacitor.

Another feature of the impedance plots is that they do not exhibit a linear region at low frequencies. The linear region probably lies at still lower frequencies at which measurements were not carried out because of large fluctuations.

3.5. Variation of conductivity with concentration of Al_2O_3 :

Fig. 3.7. shows the variation of conductivity as the concentration of alumina increases in the sample. The conductivity keeps on increasing as the amount of alumina increases and reaches a maximum at 35 m/o alumina after which it decreases. This is in

agreement with what is observed in other alkali halides. The maximum increase in conductivity is about 17 times the conductivity of pure CsBr. Higher value has been reported for other alkali halides like LiBr[29].

The conductivity enhancement can be explained by assuming alumina to act as a macro-dopant which increases the concentration of mobile point defects in the interfacial region between the dispersoid and the host material. As the concentration of alumina is slowly increased, there are more particles of alumina and hence more the number of interfaces. The host and the dispersoid form a sort of three dimensional network. Once the maximum conductivity is reached the amount of alumina present is so large that the particles of alumina come close to each other and the blocking effect of alumina predominates. Hence the conductivity starts decreasing.

Another effect observed is the dependence of conductivity on the particle size of the dispersoid. Fig. 3.8. shows the plot of normalised conductivity against the inverse of particle size of the dispersoid alumina. It is seen that as the particle size decreases the conductivity is higher. This in accordance with Jow and Wagner's theory[19] according to which the enhancement in conductivity is given by

$$\Delta\sigma = 3\ \Sigma_I e\ \mu_I < \Delta n_i > \lambda\ \frac{(r_1/r_2)^3}{[\,1 - (r_1/r_2)^3\,]} \qquad (3.3)$$

where

μ_I - mobility of the defects

$< \Delta n_i >$ - average excess charge density

λ - thickness of the space charge layer

r_1 - size of alumina particle

r_2 - half the average distance between two alumina particles

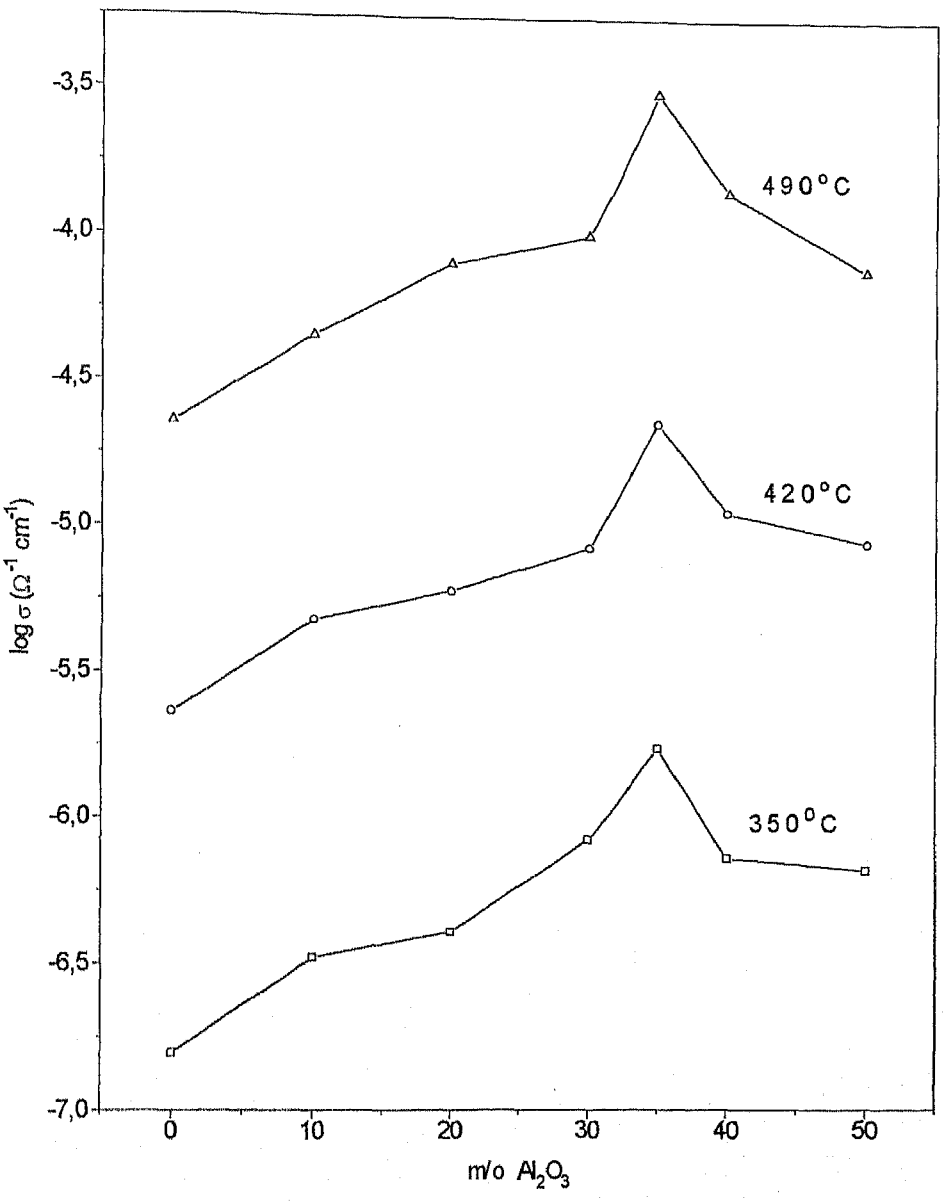

Fig. 3.7. Variation Of Conductivity with m/o Al_2O_3

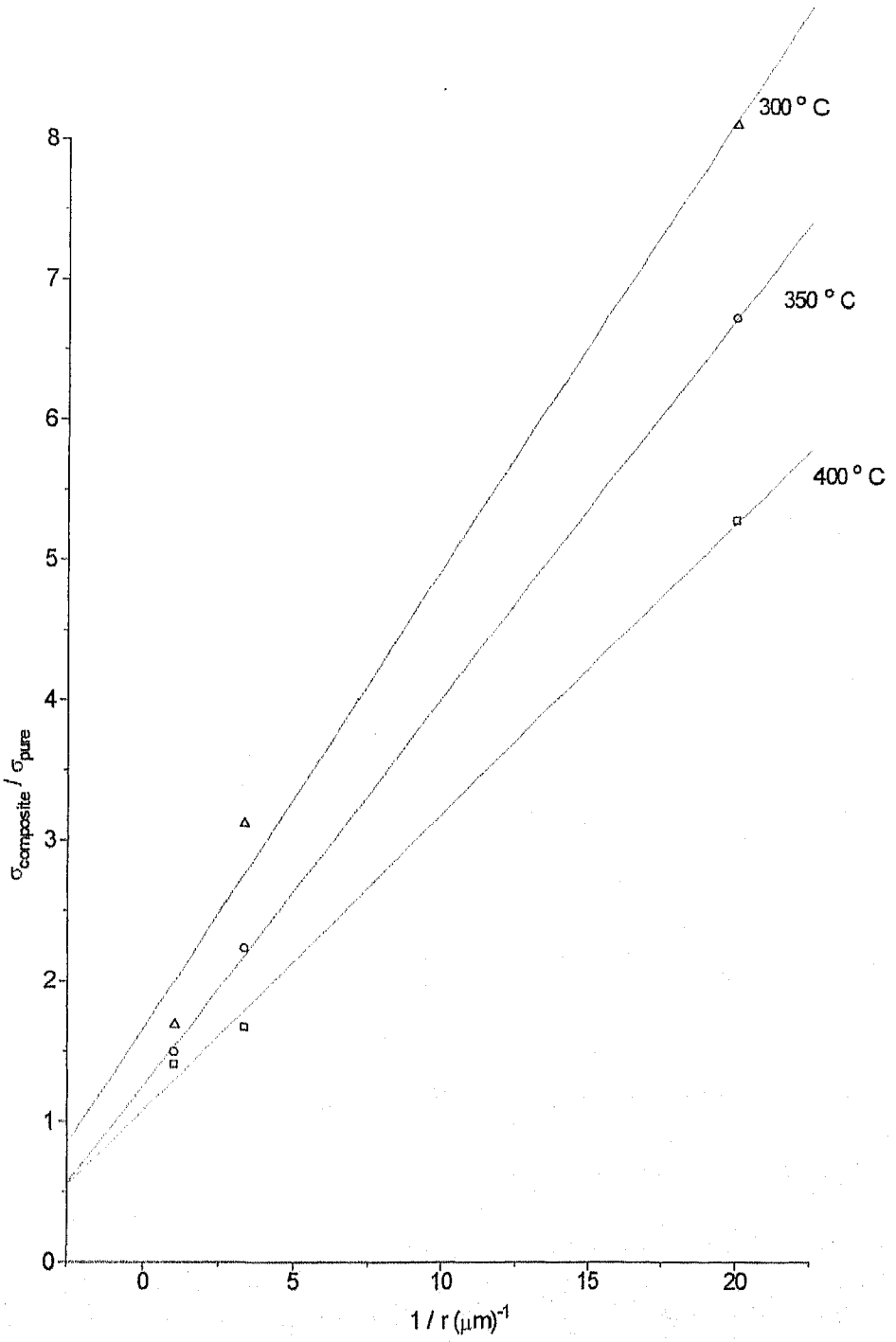

Fig. 3.8 Plot of normalised conductivity ($\sigma_{composite} / \sigma_{pure}$) vs. inverse particle size of Al_2O_3 for three different sizes viz. 0.05 μm, 0.3 μm, 1.0 μm.

In case where $r_2 >> r_1$, $(r_1/r_2)^3$ can be approximated to v_v, the volume fraction of the dispersoid. The relation (3.2) reduces to

$$\Delta\sigma = 3\ \Sigma_I\ \mu_I\ <\Delta n_i>\ \lambda\ (1 / r_1)\ [\ v_v / (1 - v_v)\ ] \qquad (3.4)$$

Since μ_I, Δn_i and λ are all functions of temperature, at one particular temperature, the excess conductivity

$$\Delta\sigma\ \alpha\ (1 / r_1)[\ v_v / (1- v_v)] \qquad (3.5)$$

Thus a plot of normalised conductivity against the inverse of particle size of alumina should be a straight line. Even though the plots are reasonably good straight lines, it needs to be stressed that unfortunately only three particle sizes of alumina were available. Nevertheless, the conclusion are fairly reliable since the data point corresponding to 0.05 micron alumina lies farther apart from the other two but still falls on the same straight line.

From the plot it can be concluded that the enhancement effect will be seen only for particles of size upto a few microns. Qualitatively the enhancement effect can be explained as follows. The number of particles of 0.05 micron size alumina present in the 30 mol. % sample will be larger than the that for 0.3 micron size alumina. The greater the number of particles, the greater will be the effective interface between dispersoid and host. Hence, the concentration of mobile defects produced will also be higher leading to better enhancement in conductivity. However, if the particle size becomes too large, say of the order of a few microns, the blocking effect of the insulator starts exhibiting itself and the conductivity may become less than that of the pure sample.

3.6. Variation of conductivity with temperature :

Figs. 3.9 - 3.11 show the variation of conductivity with temperature. Fig. 3.9 and 3.10. show the plots for pure, 10, 20, 30, 35, 40 and 50 m/o dispersions of 0.05 μm alumina. Fig. 3.11. shows the plots for 30 m/o dispersion of 0.05 μm, 0.3 μm alumina and 1.0μm alumina. Strictly, only log (σT) should vary linearly with inverse of temperature. However, for reasons stated in Section. 1.4., even a plot of log σ against 1/T is also linear to a good approximation under experimental conditions.

The extrinsic and intrinsic regions can be clearly seen. The demarcation between the two regions gives the knee temperature. The extrinsic region is governed by the equation of straight line

$$A_1 \exp(-E_a / (kT))$$

The intrinsic region is governed by the equation

$$A_2 \exp(-E_a' / (kT)).$$

where

E_a - Activation energy for migration of defects (H_m)

E_a' - Sum of the activation energy for migration and half the activation energy of formation of defects ($H_m + H_s / 2$)

So knowing the slopes of the two regions, the energy required for migration and formation of defects can be deduced. The activation energy is a very important factor. This is so because it is only the activation energy which decides whether a particular solid electrolyte can be utilised in the fabrication of a practical solid state battery. Materials with low activation energies are preferred for use in high-energy density batteries.

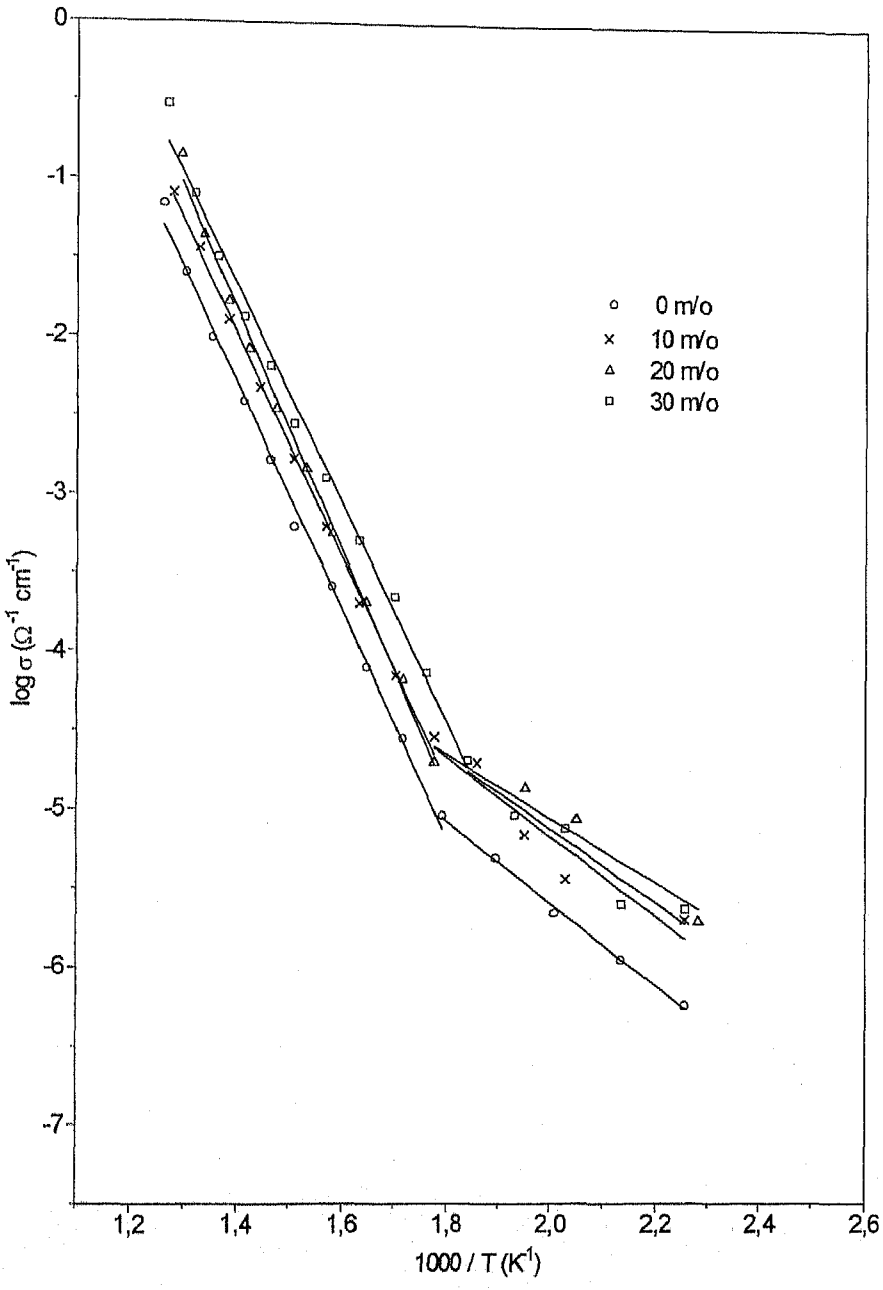

Fig. 3.9. Arrhenius plots for different m/o dispersions of 0.05 μm Al_2O_3

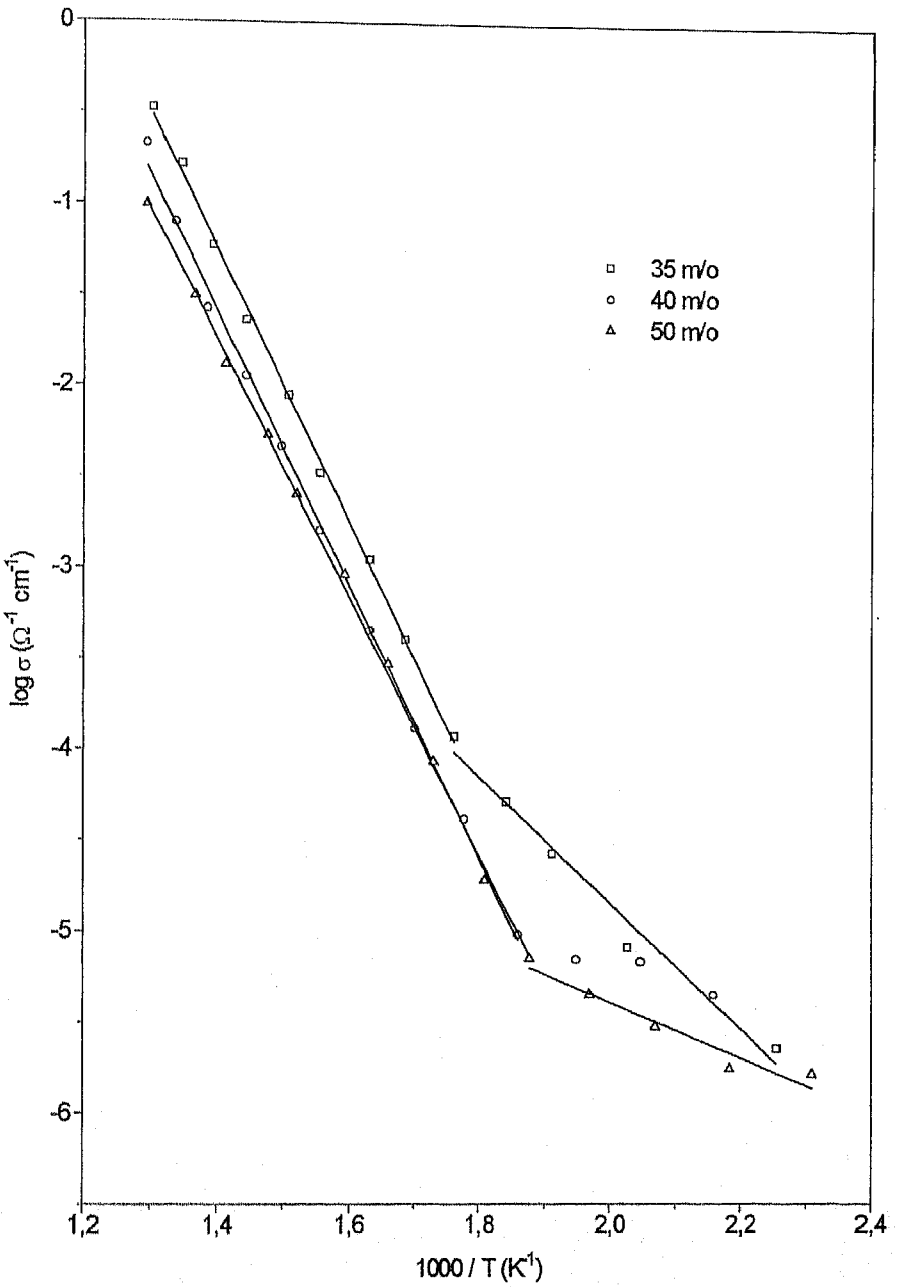

Fig. 3.10. Arrhenius plots for different m/o dispersions of 0.05 μm alumina

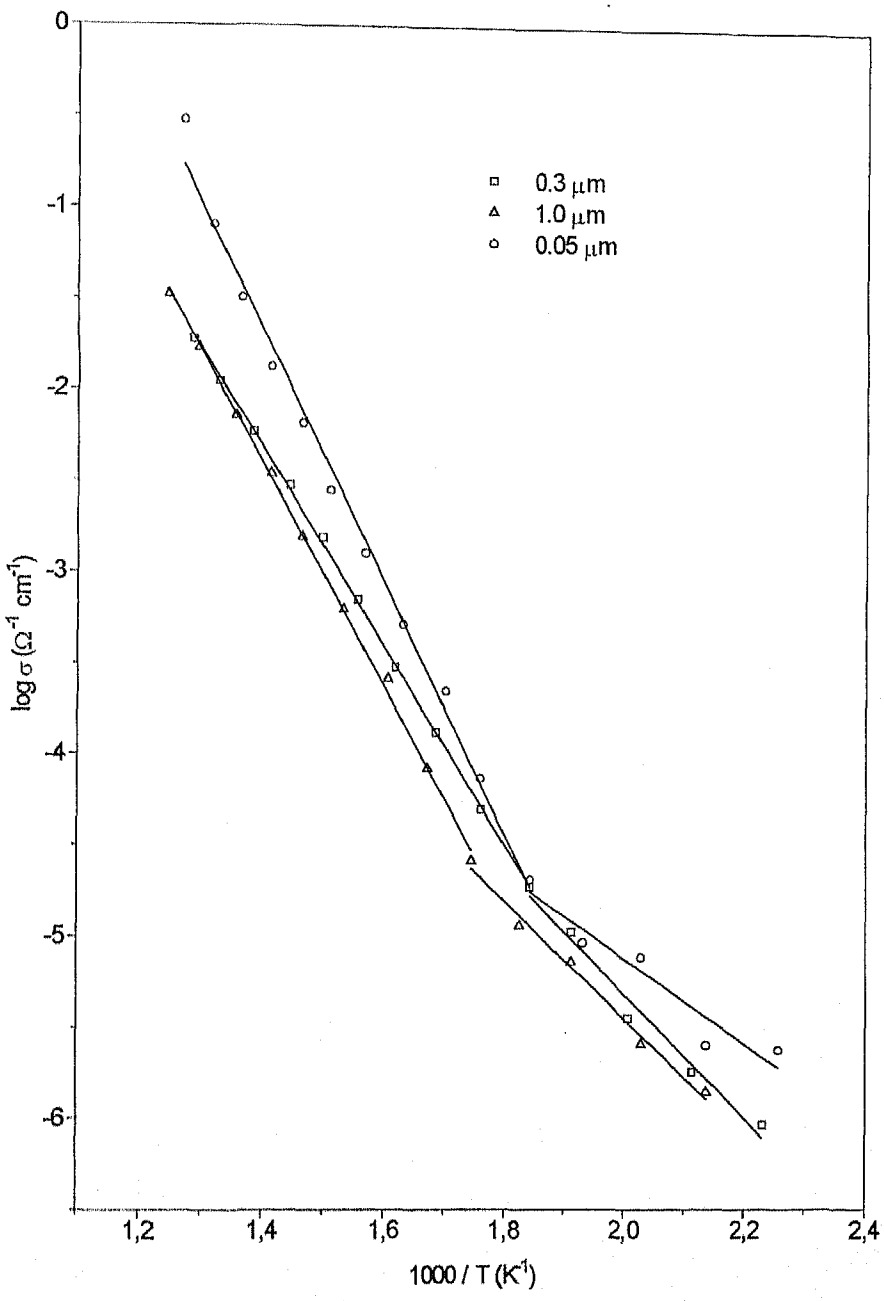

Fig. 3.11. Arrhenius plots for 30 m/o Al_2O_3 samples with different particle sizes of alumina

Table 3.1.

Activation Energies of Different Samples

alumina m/o	slope extrinsic (H_m) eV	slope intrinsic ($H_s/2 + H_m$) eV	H_s eV
0	0.52	1.43	1.82
0[30]	-	1.44	-
10	0.50	1.40	1.81
20	0.40	1.52	2.23
30	0.46	1.37	1.82
35	0.69	1.49	1.60
40	-	1.49	-
50	0.31	1.41	2.21

Table 3.2.

Pre-Exponential Factors and Knee Temperatures For Different Samples

alumina m/o	σ_o (Ω^{-1} cm^{-1})	Knee Temperature ($^{\circ}$ C)
0	4.66×10^4	285
0[130]	2.50×10^4	-
10	8.85×10^4	290
20	7.68×10^5	290
30	1.04×10^5	280
35	1.73×10^6	295
40	8.47×10^5	-
50	1.52×10^5	260

Table 3.1. gives the activation energies for formation and migration of defects. Table 3.2. lists the pre-exponential factors along with the knee temperatures. It may be pointed out that the activation energy and pre-exponential factor obtained for CsBr is in good agreement to the values reported in the literature. As already mentioned in Section 1.4. the knee temperature is a measure of the purity of or impurity present in the material. As we are adding more and more alumina, it creates mobile point defects which are responsible for the enhancement in conductivity. So, one would expect that the extrinsic region would be enlarged and the knee temperature shifted to a higher value. When the curves for pure and 35 m/o dispersed alumina are compared, a slight shift can be perceived. However, it is not so obvious for lesser concentrations of alumina. This maybe because the enhancement in conductivity is not sufficiently high for low concentrations of alumina which means that not a large number of point defects are produced. As a result, the shift in the knee towards higher temperature is not clearly seen.

It must be mentioned that the transition from extrinsic to intrinsic is expected to be gradual rather than abrupt. So, the knee temperatures listed in Table 3.1 are only approximations.

CsBr exhibits schottky type of defect in which the anion vacancies are more mobile[31]. Strictly, the value of H_s, the energy of formation of defects, should be a constant for all concentrations. It is seen from Table 3.1. that the slope of the intrinsic region is nearly constant for all samples. However, because of the limitations of the measuring instrument at low temperatures, the values obtained in the extrinsic region are not highly reproducible. Hence, variations are seen in the values of H_s. It is seen that there is an increase in the activation energy for 35 m/o alumina dispersion. This suggests that as

the concentration of alumina increases the conductivity is dominated by Cs^+ ion vacancies which have a higher activation energy[32].

3.7. Summary And Conclusions :

(1) In all, nine different composite solid electrolyte samples were prepared viz. CsBr (pure), CsBr-10 m/o, 20 m/o, 30 m/o, 35 m/o, 40 m/o, 50 m/o Al_2O_3 (0.05 μm particle size); CsBr-30 m/o Al_2O_3 (0.3 μm particle size); CsBr-30 m/o Al_2O_3 (1.0 μm particle size).

(2) All the samples were investigated by XRD and DTA to verify the melting point and to check if any new phase or solid solution formation has occurred.

(3) All the samples were subjected to impedance analysis for the determination of conductivity and activation energies for ion transport.

(4) There is a marked enhancement in the conductivity of CsBr due to alumina dispersion. The maximum enhancement is observed at 35 m/o Al_2O_3 which is about 15 times that of pure CsBr. Also the enhancement in conductivity varies inversely with the particle size of alumina used.

(5) The above results are similar to those obtained for other alkali halides and can be satisfactorily explained by the space charge theory.

REFERENCES

1) Faraday M (1839) in : Experimental investigtions in electricity, Quartich, London; no. 1340.

2) Takahashi T (1986) in : "Materials for solid state batteries ", ed. by Chowdari B. V. R. and Radhakrishna S, World Sci. Publ. Co., Singapore.

3) Suresh Chandra (1981), "Superionic Solids", North - Holland Publ. Co., p20.

4) Ravaine D (1980), J. of Non - Crystalline Solids,38/39, 353.

5) Minami T (1985), J. of non - crystalline solids, 73, 273 - 284.

6) Shiuli Gupta (1994), "Ph. D thesis on Ionic Transport in PEG - MX polymeric electrolytes ", p 162

7) Liang C C (1973), J. of Electrochem. Soc., 120, 1289.

8) Jow T and Wagner J B Jr. (1979), J. Electrochem. Soc., 126, 1963.

9) Shahi K and Wagner J B Jr. (1982), J. of Solid State Chem., 42, 107.

10) Maier J (1985), Mat. Res. Bull.,20, 383.

11) Fijitsu S, Kuomoto K and Yanagida H(1986), Solid State Ionics , 18/19, 1146.

12) Vaidehi N, Akila R, Shukla A K and Jacob K T (1986), Mat. Res. Bull. 21, 909.

13) Ashok Kumar and Shahi K (1994), Bull. of Mat. Sc., vol. 17, no. 3, 209 - 217.

14) Agrawal R C and Gupta R K (1995), J. of Mat. Sc., 30, 3612 - 3618.

15) Liang C C, Joshi A V and Hamilton N E (1978), J. of Appl. Electrochem., 8, 445.

16) Stoneham A M, Evelyn Wade and Kilbur J A (1979), M. Res. Bull., 14, 661.

17) Jacobs P W M and Tompkins F C (1952), Q. Rev. Chem. Soc., 6, 238.

18) Maxwell J C (1881) in : " A Treatise on electricity and magnetism", vol. 1, 2nd ed., Clare Don Pres, Oxford, p 435.

19) Jow T and Wagner J B Jr. (1975), J. of electrochemical Soc., 126, 1963.

20) Maier J (1985), J. of Phy. Chem. of solids, vol. 46, no. 3, 309 - 320.

21) Roman H E, Bunde A and Dietrich W (1986), Phy. Rev. B, vol. 34, no. 5, 3439 - 3445.

22) Bauerle J E (1969), J. Of Phy. Chem. Solids, 30, 2657.

23) Archer W I and Armstrong R D (1980) in : Electrochemistry vol. 7, ed. Thirsk H R, The Chem. Soc., London, p 157.

24) Hooper A (1977), J. Phys. D, 10, 1487.

25) Macdonald J R (1984), Solid State Ionics, 18/19, 147.

26) Raistrick I D (1986), Solid State Ionics, 18/19, 40.

27) Bunde A, Dietrich W and Roman H E (1985), Phys. Rev. Lett., 55, 5.

28) Wang J C and Dudney N J (1986), Solid State Ionics, 18/19, 112.

29) Lynch D W (1960), Phys. Rev. 118, 468.

30) Shiuli Gupta (1986), "M. Tech Thesis on Enhanced Electrical transport in LiBr-Al_2O_3 multiphae mixture".

31) Hladik J (ed.) (1972), "Phys. Of Electrolytes", Acad. Press, vol.1 p199.

32) Harvey D J and Hoodless I M (1967), Phil. Mag. 16, 543.